https://doi.org/10.5194/egusphere-2026-7153
Preprint. Discussion started: 24 November 2026
© Author(s) 2026. CC BY 4.0 License.

A climatological perspective on the seasonal and regional water vapor variability in the UT/LS from air- and balloon-borne in-situ measurements

Patrick Konjari[1], Christian Rolf[1], Hans-Christoph Lachnitt[2], Susanne Rohs[3], Andreas Petzold[3,5], Harald Bönisch[4], Andreas Zahn[4], Paul Konopka[1], and Peter Hoor[2]

[1]Forschungszentrum Jülich GmbH, Institute of Climate and Energy Systems 4 – Stratosphere, Jülich, Germany
[2]Johannes Gutenberg-Universität Mainz, IPA, Mainz, Germany
[3]Forschungszentrum Jülich GmbH, Institute of Climate and Energy Systems 3 – Troposphere, Jülich, Germany
[4]Karlsruhe Institute of Technology, Institute of Meteorology and Climate Research, Karlsruhe, Germany
[5]Bergische Universität Wuppertal, Institute for Atmospheric and Environmental Research, Wuppertal, Germany

Correspondence: Patrick Konjari (p.konjari@fz-juelich.de) and Christian Rolf (c.rolf@fz-juelich.de)

Abstract. Water vapor in the upper troposphere and lower stratosphere (UT/LS) strongly influences the thermodynamic structure of the atmosphere, with impacts extending to the surface. Quantifying its radiative effects remains challenging due to substantial observational uncertainties. To address this, we analyze airborne campaign and balloon-borne observations alongside the adjusted IAGOS water vapor dataset, comprising approximately 70,000 passenger aircraft flights, to investigate UT/LS water vapor variability.

The observations reveal a pronounced seasonal cycle in both the extratropical UT and LS. In the UT and extratropical transition layer (exTL), water vapor seasonality closely follows temperature and tropopause height, with maximum mixing ratios in July and August. Above the exTL, mixing ratios peak in fall; at 100 hPa, they increase from approximately 4 to 5.5 ppmv.

In the lower exTL, where relatively rapid mixing processes dominate, distinct geographical differences emerge from the adjusted IAGOS data. Among well-sampled regions (North America, the Atlantic, Europe, and Asia), the Atlantic sector is significantly moister below 340 K during winter. Convective moistening associated with summer monsoon regions is evident in the adjusted IAGOS data only in the UT, likely reflecting the relatively low sampling altitudes. In contrast, higher-reaching balloon-borne observations reveal a pronounced summer increase in water vapor over North America compared with Europe.

https://doi.org/10.5194/egusphere-2026-7153
Preprint. Discussion started: 24 November 2026
© Author(s) 2026. CC BY 4.0 License.

1 Introduction

In the upper troposphere and lower stratosphere (UT/LS), water vapor (H_2O_{gas}) has a significant impact on the global climate system (IPCC, 2023). Because the UT/LS is cold and dry (Zahn et al., 2014), even small increases in H_2O_{gas} significantly reduce outgoing longwave radiation from the Earth to space (Riese et al., 2012; Solomon et al., 2010), thereby significantly affecting the local temperature structure by enhancing radiative cooling within the UT/LS (Riese et al., 2012; Banerjee et al., 2019; Gettelman et al., 2011). This cooling at high altitudes alters the vertical temperature gradient and leads to a slight warming of the surface and the troposphere below, as less longwave radiation escapes to space and more energy is retained within the lower atmosphere. For the future, most global climate models predict an increase in stratospheric H_2O_{gas} and a corresponding total stratospheric H_2O_{gas} radiative feedback parameter of 0.1 – 0.3 W m-2 per 1 Kelvin of surface warming (e.g., Banerjee et al., 2019; Huang et al., 2020).

UT/LS H_2O_{gas} shows significant variations both seasonally and geographically, as well as from year to year. This is, for example, evident from Microwave Limb Sounder (MLS; Schoeberl et al., 2006) observations at 380 K potential temperature (Figure C1). The global-scale upwelling associated with the Brewer-Dobson circulation (BDC) in the tropics and the subsequent transport of air into the extratropics, with a timescale of several months at the 380 K potential temperature level (Bönisch et al., 2008), is clearly evident. Further features at this level include the influence of dehydrated air masses associated with the polar jets, particularly during Southern Hemisphere winter, as well as the hydration of dry tropical air masses in the northern extratropics during summer, especially in association with the Asian and N. American monsoon systems.

At lower levels, below 380 K, the vertical and geographical gradients in water vapor increase towards the tropopause and towards higher latitudes, where short-term mixing becomes increasingly important, in contrast to the predominantly global-scale transport processes prevailing above (Konjari et al., 2025a; Zahn et al., 2014). Here, the space-borne observations are limited by their vertical resolution of several kilometers (e.g., MLS: 2–3 km). As a result, they cannot adequately capture the strong temporal and spatial (especially vertical) variability of H_2O_{gas} across the UT/LS region (Gettelman et al., 2011; Zahn et al., 2014). Global climate models, on the other hand, have also been shown to significantly deviate from observations, especially due to an inadequate representation of UT/LS transport and mixing processes (Charlesworth et al., 2023). Figure 1 illustrates the discrepancies between in-situ observations, satellite measurements, and model data using vertical profiles from balloon-borne cryogenic frost point hygrometer (CFH) measurements from the Network for the Detection of Atmospheric Composition Change (NDACC) network, together with collocated MLS (version 6; Lambert et al., 2026) satellite measurements, ERA5 reanalysis data (Hersbach et al., 2020) and CLaMS (Chemical Lagrangian Model of the Stratosphere; McKenna et al., 2002) model simulations.

Here, a systematic dry bias of MLS is evident in parts of the UT/LS. ERA5 indicates moister conditions throughout the LS (e.g., 7.5 ppmv at 150 hPa, corresponding to a positive bias of 2 ppmv), potentially resulting from numerical diffusion and the associated overestimation of convective moistening (Konjari et al., 2025b), as well as excessive UT-LS mixing in general. In contrast, CLaMS exhibits a pronounced moist bias primarily in the UT and tropopause region. Overall, the discrepancies between the CFH observations, model data, and MLS observations imply substantial differences in the total radiative effect

https://doi.org/10.5194/egusphere-2026-7153
Preprint. Discussion started: 24 November 2026
© Author(s) 2026. CC BY 4.0 License.

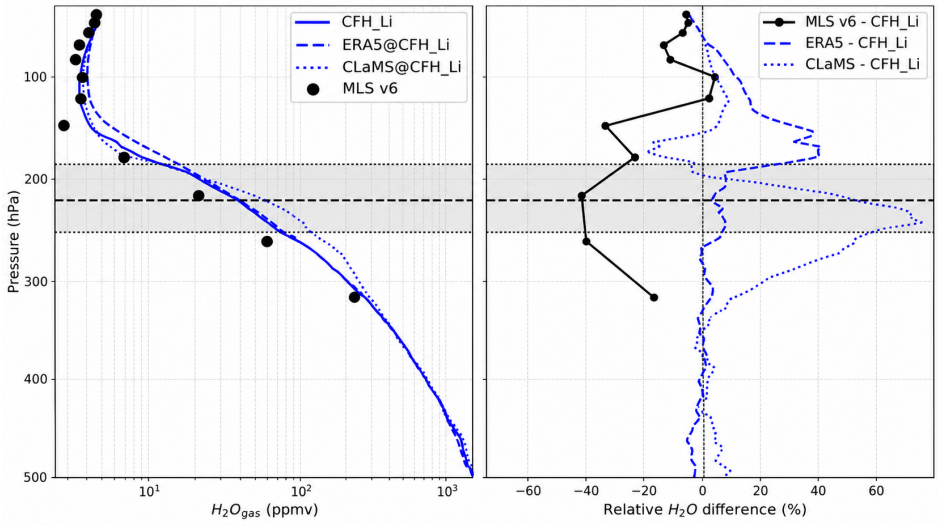

Figure 1. Intercomparison of H_2O_{gas} profiles from different datasets. (a) The blue solid line shows the mean profile from balloon-borne frost point hygrometer measurements taken over Lindenberg, Germany, in summer (June-August). In addition, collocated satellite (MLS) and model (ERA5 and CLaMS) profiles are shown. The horizontal black dashed and dotted lines indicate the mean and 10th and 90th percentile thermal tropopause levels, respectively. (b) Same as in (a) but for relative differences compared to the CFH profile.

of UT/LS H_2O_{gas}, potentially leading to UT/LS temperature differences on the order of several kelvin (Charlesworth et al., 2023).

For a better quantification of UT/LS H_2O_{gas} and its impact on the global climate system, airborne in-situ measurements are therefore essential for adequately characterizing the H_2O_{gas} variability in the UT/LS, its radiative effects, and the associated impacts on the atmospheric circulation (Charlesworth et al., 2023). In this study, the H_2O_{gas} variability in the UT/LS is quantified using a suite of air- and balloon-borne in-situ datasets. These include passenger aircraft observations from IAGOS (In-Service Aircraft for a Global Observing System; Petzold et al., 2015) collected during the MOZAIC (Measurement of Ozone and Water Vapour on Airbus In-Service Aircraft; Helten et al., 1999) and CORE project phases, as well as airborne measurements conducted within the framework of IAGOS-CARIBIC (Civil Aircraft for the Regular Investigation of the Atmosphere Based on an Instrument Container; Dyroff et al., 2015) and various other research campaigns (see Section 2). Additionally, balloon-borne frost point hygrometer measurements (e.g., over Boulder, Colorado, and Lindenberg, Germany) provided by NDACC are utilized.

In summary, based on the utilized datasets, this work aims to answer the following questions:

- How does UT/LS H_2O_{gas} vary seasonally along different (zonal) regions or measurement locations?
- What are the distinct geographical features of UT/LS H_2O_{gas}?

https://doi.org/10.5194/egusphere-2026-7153
Preprint. Discussion started: 24 November 2026
© Author(s) 2026. CC BY 4.0 License.

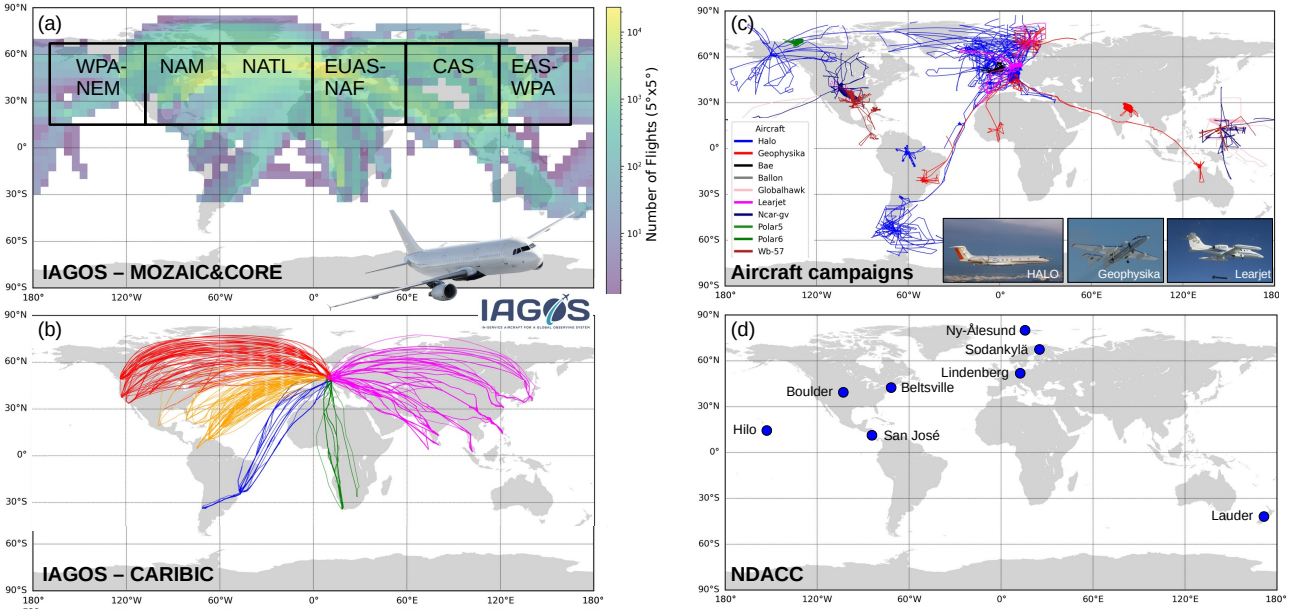

Figure 2. Data coverage. (a) Flight number density from MOZAIC&CORE data. (b) CARIBIC flight routes; different colors indicate different target regions. (c) JULIA campaign flights; flights with different research aircraft are indicated by different colors. The three most frequently used aircraft, Geophysika, HALO and Learjet, are shown at the bottom. (d) Location of the NDACC frost point hygrometer observation sites. Credits for images in (c): DLR (CC BY-NC-ND 3.0) (left), Ralf Weigel (middle), https://www.enviscope.de/airtoss/ (right, last access: 12.11.2026).

– How can observed LS H_2O_{gas} values be related to mixing processes on different scales, ranging from convection to large-scale global transport on timescales of weeks to months?

The work is structured as follows: Section 2 describes the datasets and their use in this study. In Section 3, the in-situ datasets are analyzed, providing a climatological perspective on the H_2O_{gas} variability. Specifically, the seasonal variability is examined in Section 3.1, and geographical variability is further explored in Section 3.2. A summary and discussion of the key findings is provided in Section 4.

2 In-situ datasets and data handling

In the first part of this section (Section 2.1), the in-situ datasets are presented: adjusted IAGOS-MOZAIC&CORE climatologies (Section 2.1.1), the TPChange (The Tropopause Region in a Changing Atmosphere) database (Section 2.1.2) and NDACC frost point hygrometer measurements (Section 2.1.3). The datasets are summarized in Table 1. Section 2.2 describes their spatial and temporal distribution, while Section 2.3 describes how the data are processed for the analysis.

https://doi.org/10.5194/egusphere-2026-7153
Preprint. Discussion started: 24 November 2026
© Author(s) 2026. CC BY 4.0 License.

2.1 Air- and balloon-borne in-situ datasets

The aim of this study is to combine available in-situ datasets to obtain an improved understanding of water vapor variability by exploiting and combining the complementary strengths of the individual datasets. The IAGOS-MOZAIC and -CORE observations have the advantage of providing a large number of observations from more than 70,000 passenger aircraft flights, covering the 9–12.5 km passenger aircraft flight altitude range. In a previous study by Konjari et al. (2025a), a moist bias in the IAGOS-MOZAIC and IAGOS-CORE data under dry stratospheric conditions was corrected, enabling the use of these datasets to be extended from the UT into the LS. Their extensive measurement coverage, spanning much of the Northern Hemisphere and parts of the Southern Hemisphere over a period of almost 30 years, allows for the quantification of the geographical variability of H_2O_{gas} within the sampled regions.

The campaign observations, despite providing a comparatively smaller amount of data (e.g., IAGOS-CARIBIC: approximately 500 flights and other campaigns: around 1000 flights), provide LS measurements of higher accuracy than the adjusted IAGOS-MOZAIC and -CORE data. Additionally, the campaign observations extend deeper into the LS (up to around 20 km in some cases). The IAGOS-CARIBIC and other campaign observations are merged into the TPChange dataset (from now on just TPC; Lachnitt, 2025).

The NDACC observations provide long-term records at different sites around the world. Similar to the campaign observations, their measurements are of high accuracy, even under dry stratospheric conditions (Vömel et al., 2007). Additionally, they extend deep into the stratosphere, reaching altitudes of up to around 30 km. One disadvantage is that the balloon observations

Table 1. Summary of the UT/LS airborne in-situ H_2O_{gas} datasets

Product	Instruments	Measurement Quantity	Time period	Accuracy	Reference
IAGOS-MOZAIC&CORE$_{adj}$	ICH	RH_{liq}	1995 - 2026	4 – 7 % RH_{liq}	Konjari et al. (2025a)
IAGOS-CARIBIC	WaSul-Hygro, CR-2	H_2O_{gas} VMR T_{frost}	1997 - 2020	4 %, 0.1 K	Dyroff et al. (2015)
Aircraft campaigns	FISH, SHARC, others	H_2O_{gas} VMR	1994 - 2026	5 - 7%	Zöger et al. (1999)
NDACC	Frost point hygrometer	Frost point temp.	1991 - 2026	2 - 5 %	Vömel et al. (2016)

https://doi.org/10.5194/egusphere-2026-7153
Preprint. Discussion started: 24 November 2026
© Author(s) 2026. CC BY 4.0 License.

are limited to fixed locations. Therefore, the airborne observations, especially IAGOS-MOZAIC and -CORE, which cover a much broader geographical range, are particularly important for a better quantification of the geographical variability of H_2O_{gas}.

2.1.1 IAGOS passenger aircraft observations: Adjusted MOZAIC&CORE climatologies

With their extensive spatial and temporal coverage, the IAGOS-MOZAIC&CORE observations provide a valuable basis for improving the understanding of UT/LS water vapor variability. The capacitive sensors onboard IAGOS-MOZAIC&CORE flights have been shown to perform well in moist UT air masses. However, due to adiabatic heating of the sampled air as it flows through the aircraft inlet, the sensor temperature is 20–30 K above ambient temperature, reducing the measured relative humidity (with respect to liquid water; RH_{liq}) by a factor of 5–10 (Neis et al., 2015). In the LS, RH_{liq} at the sensor can drop below 1 %, where sensor sensitivity is limited, resulting in systematic moist biases for ambient RH_{liq} values below approximately 10 % (Rolf et al., 2023; Neis et al., 2015; Konjari et al., 2025a). In order to make the large quantity of MOZAIC&CORE H_2O_{gas} data usable also for studying LS water vapor, Konjari et al. (2025a) assessed the biases in the RH_{liq} measurements and applied a bias adjustment. This adjustment is applied to climatological means, but not to individual observations. The adjusted MOZAIC&CORE climatologies are merged into a single dataset (MOZAIC&CORE$_{adj}$). The data are available on the Zenodo platform (https://zenodo.org/records/14852197; Konjari et al., 2025c, last access: 12.11.2026) on different pressure and potential temperature levels on a 5°×5° latitude–longitude grid.

The MOZAIC&CORE$_{adj}$ dataset enables a comprehensive geographical assessment of the H_2O_{gas} variability while for other datasets like TPC the limited data amount only allows for the analysis of zonal means. However, uncertainties that arise from the bias adjustment have to be kept in mind. Specifically, for mean H_2O_{gas} mixing ratios mostly below 20–30 ppmv (corresponding to RH_{liq}<30 %), mean values tend to be biased and are adjusted. Overall relative uncertainties of adjusted mean values are in the range of 10-20 % for most mean values with H_2O_{gas}>10 ppmv but can increase to up to 30 % for lower mixing ratios (Konjari et al., 2025a).

2.1.2 Airborne campaign observations: The TPChange dataset

Within the framework of the DFG Collaborative Research Center TPChange (Tropopause Region in a Changing Atmosphere; https://tpchange.de/) a merged in-situ dataset was produced from various airborne measurement campaigns that are summarized in JULIA (Jülich in-situ database) as well as passenger aircraft observations from IAGOS-CARIBIC (Civil Aircraft for the Regular Investigation of the Atmosphere Based on an Instrument Container; Dyroff et al., 2015).

The measurement campaigns provide data from over 1,100 research aircraft flights conducted during 49 campaigns carried out since 1994. JULIA provides observations of trace gases like H_2O_{gas} and O_3, and cloud microphysical properties. H_2O_{gas} data are provided by instruments that have a high sensitivity to low stratospheric H_2O_{gas} concentrations, with the largest quantity of the measurements being performed by the Fast In-situ Stratospheric Hygrometer (FISH; Zöger et al., 1999).

IAGOS-CARIBIC (from now on just CARIBIC), operating from 1997 to 2020 and consisting of around 500 long-distance measurement flights, provides sophisticated, research-grade instrumentation to measure over 100 atmospheric parameters,

https://doi.org/10.5194/egusphere-2026-7153
Preprint. Discussion started: 24 November 2026
© Author(s) 2026. CC BY 4.0 License.

including a wide range of trace gases, isotopes, and aerosol properties. The H_2O_{gas} measurements during CARIBIC flights were performed using a dedicated measurement package that combines two instruments: the cryogenic hygrometer CR-2 and the photoacoustic hygrometer (WaSul-Hygro; Szakáll et al., 2020). The two instruments complement each other: the CR-2 provides highly accurate measurements, but with limited temporal resolution, while WaSul-Hygro has a fast response time, with measurements provided every second (or at 1 Hz). The CR-2 data are used to calibrate the WaSul-Hygro measurements for each individual flight.

2.1.3 Balloon-born frost point hygrometer measurements: NDACC

The NDACC (Network for the Detection of Atmospheric Composition Change; https://ndacc.larc.nasa.gov/data; last access: 12.11.2026) database provides balloon-borne frost point hygrometer observations from various locations around the world (see Section 2.2). The frost point hygrometers use a chilled-mirror feedback system. A small mirror is cooled with a cryogenic refrigerant until a thin layer of frost forms on its surface. An optical sensor continuously monitors the frost layer, while a feedback-controlled microprocessor adjusts the mirror temperature to maintain equilibrium between frost deposition and sublimation. The resulting frost point temperature has a temperature accuracy better than 0.2 K, and the overall uncertainty of the derived mixing ratios is on the order of 2-5 % (Vömel et al., 2016).

2.2 Temporal and spatial coverage of the in-situ datasets

The MOZAIC&CORE$_{adj}$ as well as the TPC dataset provide around three decades of data coverage, spanning from the 1990s to the 2020s (see Table 1). Geographically, the passenger aircraft (MOZAIC&CORE and CARIBIC; Figure 2a&b) predominantly cover northern mid-latitude routes, especially between N. America, Europe, and Asia. These passenger aircraft typically cruise at altitudes between 9 and 12.5 km, thereby covering the potential temperature range of 300 to 360 K (in exceptional cases up to 370 K).

In thermal tropopause-relative coordinates, passenger aircraft measurements occasionally extend up to 5 km above the tropopause in the extratropics (Konjari et al., 2025a), especially during winter and also during summer in connection with tropopause folding events, enabling sampling of deep stratospheric air masses. In tropical regions, however, measurements are generally confined to the troposphere.

In contrast to the passenger aircraft flights, data from the JULIA database (Figure 2c) reach deeper into the stratosphere and also cover the tropical UT/LS since they include research aircraft data with higher flight ceilings (e.g., Geophysika research aircraft, up to 20 km). Most of the research flights are distributed over Europe, the N. Atlantic and N. America. However, campaigns from all over the world are included.

The frost point hygrometer data from the NDACC network (Figure 2d) includes stations at Lindenberg (Germany), Boulder (Colorado, United States), Sodankylä (Finland), Ny-Ålesund (Norway), Lauder (New Zealand), San José (Costa Rica), Hilo (Hawaii, United States), and Beltsville (Maryland, United States). Among these, the Boulder station provides the longest continuous records, spanning approximately 1991 to today, while the Lindenberg, Lauder and San Jose stations have maintained regular observations from the early 2000s to today. The other stations provide shorter or discontinuous time series.

https://doi.org/10.5194/egusphere-2026-7153
Preprint. Discussion started: 24 November 2026
© Author(s) 2026. CC BY 4.0 License.

2.3 Data handling

This section describes the additional processing applied to the datasets for the analyses presented in this study. Section 2.3.1 outlines the approach used to determine the regional variability of water vapor, while Section 2.3.2 describes the merging of the TPC and NDACC frost point hygrometer datasets to create the combined TPC&NDACC dataset.

2.3.1 Determination of the geographical variability of water vapor from MOZAIC&CORE$_{\mathrm{adj}}$

For the investigation of the geographical variability, several sub-regions are defined (see Figure 2a) and compared to each other: E. Pacific–NW. America (EPAC–NWAM; 100–140°W), N. America (NAM; 60–100°W), the Atlantic (ATL; 0–60°W), Eurasia–N. Africa (EU–NAF; 0–60°E), C. Asia (CAS; 60–100°E), and E. Asia–W. Pacific (EAS–WPAC; 100–140°E). In the comparison of different geographical regions, to reduce the influence of large-scale dynamical variability, the data are also analyzed in potential temperature (Theta) and equivalent latitude (EQLat) coordinates. A regional comparison across all defined regions is possible using the MOZAIC&CORE$_{\mathrm{adj}}$ dataset. Although the TPC&NDACC dataset provides less comprehensive spatial coverage, it can nevertheless be used to assess differences between selected regions, such as Europe and N. America.

For the assessment of regional differences based on MOZAIC&CORE$_{\mathrm{adj}}$ climatologies, a key challenge in comparing different regions is the temporal inhomogeneity of the observational coverage between the regions. Since the applied adjustment requires sufficient data density, only multi-annual averages are considered (Konjari et al., 2025a). However, meaningful inter-regional comparisons additionally require comparable temporal sampling, because of the strong inter-annual variability of UT/LS water vapor (Figure B1). While the temporal coverage is relatively similar across the years spanned by the dataset for the N. Atlantic, Europe, and N. America (not shown), it differs markedly from that of the Asian regions.

Therefore, the impact of temporal inhomogeneity on intercomparisons between different regions was assessed, with the method presented in Section A. Overall, the differing temporal coverage leads to minor differences in the climatological means of the respective regions, and the main features and regional contrasts remain unchanged (not shown). Hence, in the following analyses, the data are used as given for the intercomparison rather than being homogenized.

2.3.2 Merging of TPC and NDACC frost point hygrometer observations

For the TPC dataset, the zonally averaged data provide good coverage in the Northern Hemisphere extratropics below approximately 12 km (200 hPa). At these altitudes, CARIBIC provides a substantial amount of data, and nearly all other campaign observations also reach this level. Above 12 km, however, only a subset of campaign aircraft exceed this altitude range, including HALO (14–15 km or 100 hPa) and Geophysika (20 km or 50 hPa). Consequently, the observational coverage above approximately 12 km (around 200 hPa) becomes temporally inhomogeneous. This is illustrated by the time series shown in Figure C2 (121, 147, 178, 216 hPa) which shows, on different pressure levels, monthly mean H_2O_{gas} from TPC as well as from NDACC and MLS.

For the analysis of water vapor distributions, the TPC dataset is therefore combined with NDACC observations (hereafter referred to as TPC&NDACC), which substantially increases the data coverage above 12 km. Since the NDACC observations

https://doi.org/10.5194/egusphere-2026-7153
Preprint. Discussion started: 24 November 2026
© Author(s) 2026. CC BY 4.0 License.

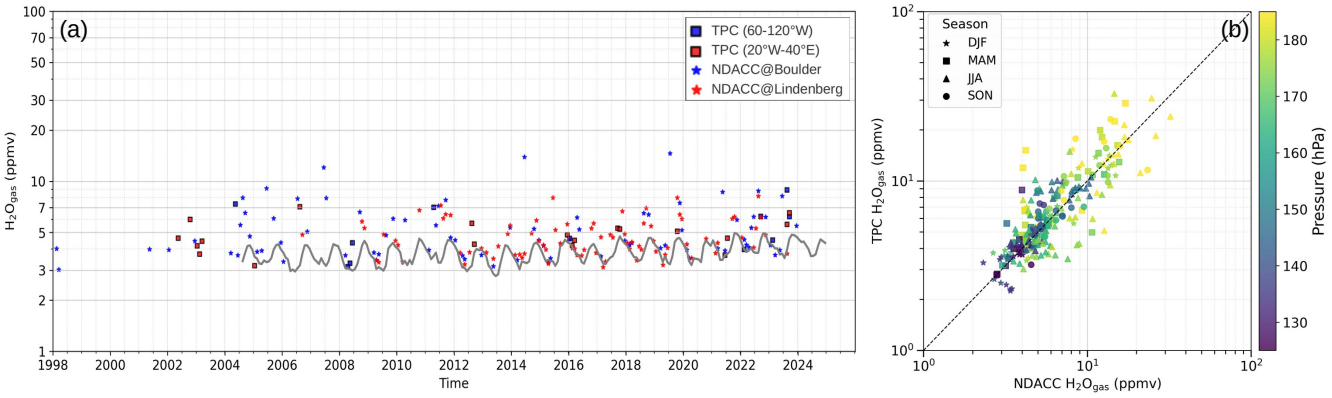

Figure 3. Comparison of NDACC and TPC. (a) Time series at 150 hPa and 50-55°N EQLat, of MLS v6 zonal mean (grey solid line), balloon-borne observations over Boulder and Lindenberg (blue and red stars, respectively), as well as TPC data sampled over 60°-120°W and 20°W-40°E (blue and red squares, respectively). (b) Monthly mean frost point hydrometer data from all stations and the TPC data are sampled in 10 hPa pressure, 5° EQLat and 20° longitude bins and are scattered against each other. The different markers indicate different seasons, and the colors indicate the pressure levels.

are limited to fixed measurement sites and TPC data above 12 km mostly come from campaign observations over Europe, however, it is important to assess how their inhomogeneous geographical sampling influences the resulting climatological perspective.

As shown in Figure 3a and Figure C2, monthly mean frost point hygrometer observations from Boulder exhibit systematically higher summertime H_2O_{gas} mixing ratios in the LS than those from Lindenberg. These discrepancies persist when using potential temperature instead of pressure as a vertical coordinate (not shown). This demonstrates that sampling moisture-related quantities in EQLat-Theta-bins does not fully eliminate discrepancies between data sets due to the non-dynamical processes affecting moisture (such as dehydration, rehydration, overshoots), which vary geographically and are affected by differences in sampling. Consequently, zonal mean values derived from the in-situ datasets are affected by geographically inhomogeneous sampling and may therefore differ from a "true" zonal mean. As a note for future intercomparison studies, this limitation should be taken into account when comparing the in-situ datasets with one another, with satellite observations or model data. In this study, rather than relying solely on zonal means based on all available observations, the analysis is performed separately for different geographical regions whenever possible. Zonal mean analyses are also included, but their interpretation accounts for the potential influence of sampling biases.

To determine if inhomogeneities persist when also considering different longitudinal regions, in a further comparison (Figure 3b), both TPC and NDACC observations were first sampled onto a common pressure–EQLat (10 hPa and 5°, respectively) grid and subsequently binned by longitude (20°) to account for differences in the geographical coverage. The data now scatter closely around the 1:1 line, indicating that binning into those coordinates minimizes sampling differences (e.g., targeted aircraft campaigns and balloon launches during suitable weather conditions, different geographical coverage).

https://doi.org/10.5194/egusphere-2026-7153
Preprint. Discussion started: 24 November 2026
© Author(s) 2026. CC BY 4.0 License.

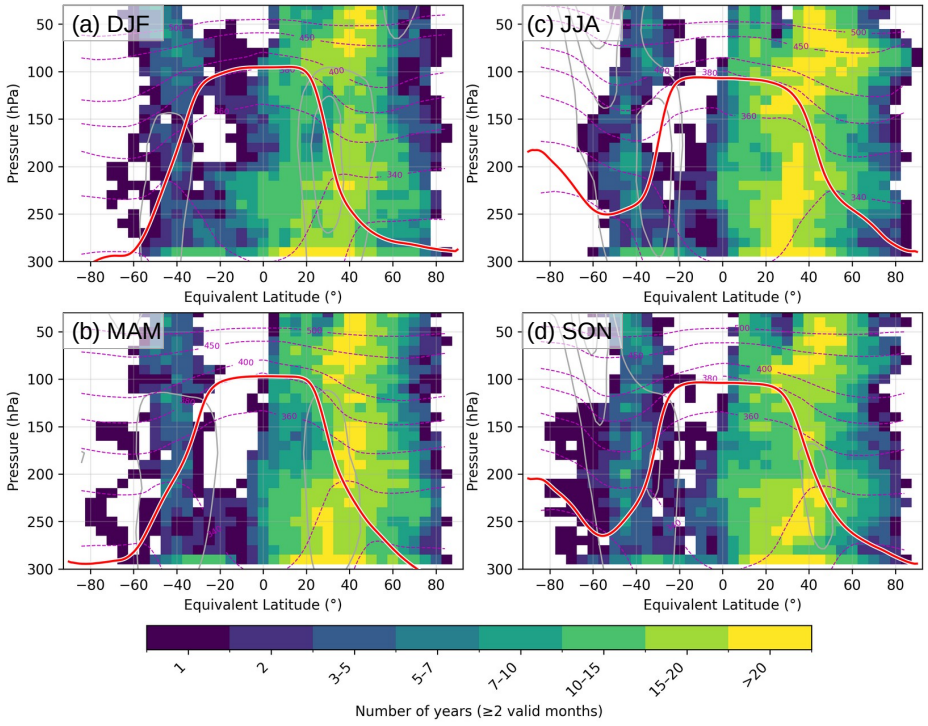

Figure 4. Seasonal cross sections of coverage from TPC&NDACC. The number of years where at least two out of three months of a season provide observations are shown. The red line indicates the mean thermal tropopause, and light gray and magenta lines wind (20, 30, 40 m/s) and potential temperature contours.

Based on merged TPC&NDACC data, seasonal and monthly means are derived by first calculating the seasonal means and monthly means for each year separately and then computing the multi-annual average from those. This is done to avoid uneven weighting of data from different years and to provide a more meaningful multi-annual mean. For seasonal means, at least 2 of the 3 months of the year must provide a valid mean value to avoid over-weighting a single month in the seasonal mean, since UT/LS H_2O_{gas} shows significant seasonal variability already on monthly scales (Konjari et al., 2025a).

For the merged dataset, when looking into zonal means the number of years in which at least two out of three months provide observations within each pressure–EQLat bin is shown in Figure 4. The Northern Hemisphere exhibits good zonal coverage, with most bins containing more than ten years of observations. In contrast, the Southern Hemisphere is generally sparsely sampled. The main exception is the 40–60°S latitude band, where good coverage is provided primarily by frost point hygrometer observations from Lauder, New Zealand.

In the Northern Hemisphere, when instead of zonal means only data from geographical regions are considered (not shown), over both N. America and Eurasia, very good coverage persists while only few observations are available from the Asian region or the oceanic regions (except for the Atlantic above 200 hPa where CARIBIC and JULIA observations contribute

https://doi.org/10.5194/egusphere-2026-7153
Preprint. Discussion started: 24 November 2026
© Author(s) 2026. CC BY 4.0 License.

to good coverage). In the Southern Hemisphere, the data come from frost point hygrometer observations over Lauder, New Zealand and campaign observations from South America and Australia (Figure 2c).

Finally, to assess the sensitivity of the monthly and seasonal means to the amount of available data, a bootstrap analysis was performed (Appendix B). For this purpose, MLS monthly means sampled in EQLat bins were used. The analysis assumes that, when sampled in EQLat, variability is dominated by diabatic processes acting on monthly or longer timescales. This is a reasonable approximation above the tropical and extratropical transition layers, where large-scale transport on the timescale of weeks to years is the primary driver of changes in H_2O_{gas} (Butchart, 2014). Under this assumption, even a limited number of flights within a given month and year can provide a representative estimate of the monthly mean. This assumption may, however, not hold in regions strongly influenced by deep convection. For example, over N. America, overshooting convection has been shown to penetrate above 400 K in extreme cases, introducing substantial short-term variability that may not be adequately captured by sparse sampling.

The analysis shows that above 400 K (corresponding to approximately 100 hPa), only about 1–2 years of observations are generally sufficient to estimate the multi-annual seasonal mean to within 10%, with at least 90% confidence. This required sampling period is substantially shorter than the observational record available over most of the Northern Hemisphere and even parts of the extratropical Southern Hemisphere. Possible exceptions are the tropical and summertime subtropical regions, where enhanced convective variability may require longer sampling periods than suggested by the bootstrap analysis. Consequently, the TPC&NDACC observational coverage in the tropical and subtropical Southern Hemisphere is likely insufficient to derive robust climatological means.

3 In-situ water vapor climatologies

In this section, the variability of H_2O_{gas} in the UT/LS is analyzed using the available in-situ datasets. In Section 3.1, the seasonal behavior is quantified using the TPC&NDACC dataset in combination with MOZAIC&CORE$_{adj}$. Because of its extensive geographical coverage, the MOZAIC&CORE$_{adj}$ dataset enables a detailed assessment of the geographical variability of H_2O_{gas}; the corresponding results are presented in Section 3.2. In contrast, the TPC&NDACC dataset is primarily used to provide a broader, zonal perspective on water vapor, benefiting from its greater vertical coverage into the LS and its higher accuracy for LS H_2O_{gas} concentrations. In addition, observations from the Northern Hemisphere mid-latitude NDACC stations with long-term records, Boulder (Colorado) and Lindenberg (Germany), are compared to investigate the local influence of convective moistening associated with the North American monsoon over Boulder.

3.1 The seasonality of UT/LS water vapor

Figure 5 shows zonal mean H_2O_{gas} sampled in pressure–EQLat space based on the TPC&NDACC data. Additionally, Figure 6 shows the seasonal cycle of mean H_2O_{gas} versus pressure for different EQLat ranges, and Figure 7 shows the corresponding seasonal mean tracer–tracer correlations between H_2O_{gas} and O_3 from TPC data for two EQLat bands. Because zonal means derived from geographically inhomogeneous observations may be affected by sampling biases (as discussed in Section 2.3.2),

https://doi.org/10.5194/egusphere-2026-7153
Preprint. Discussion started: 24 November 2026
© Author(s) 2026. CC BY 4.0 License.

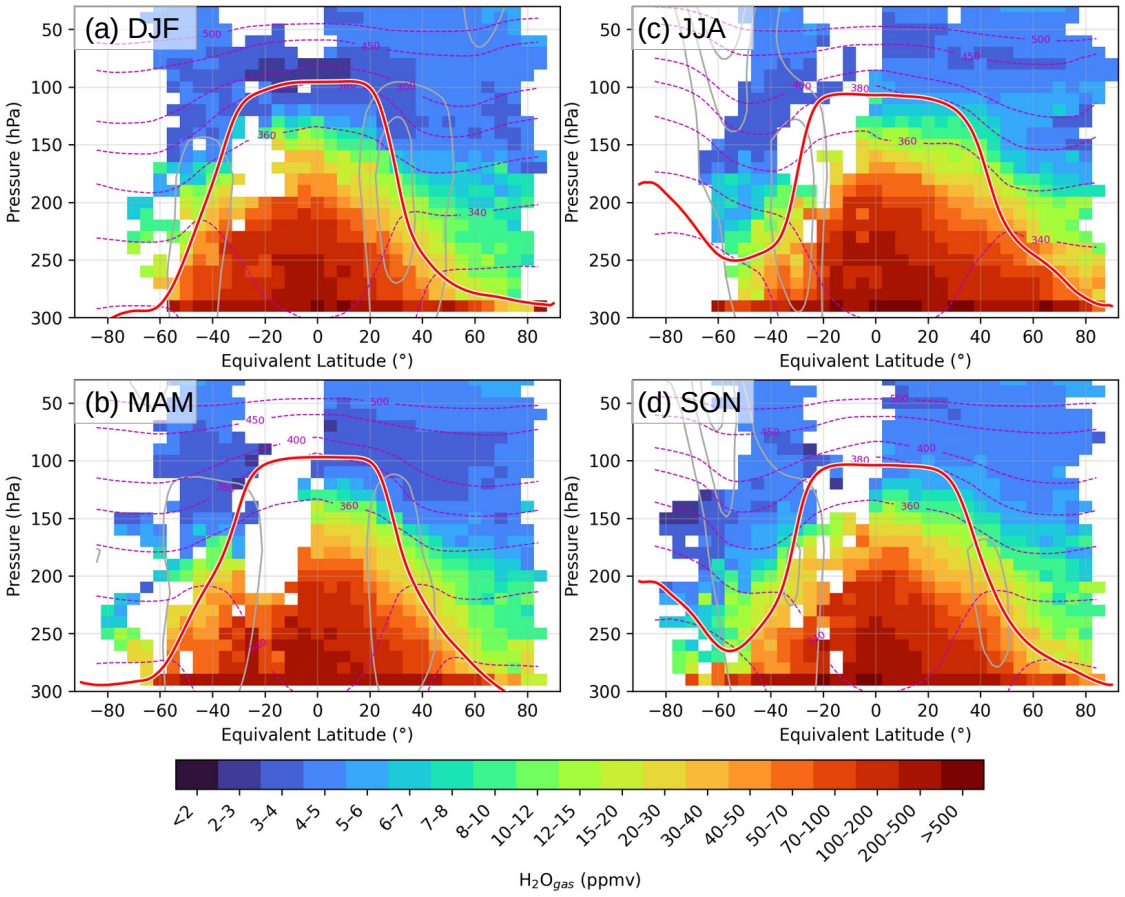

Figure 5. H_2O_{gas} cross section from TPC&NDACC observations. Seasonal mean H_2O_{gas} is shown in Pressure-EQLat coordinates. The red line indicates the mean position of the thermal tropopause derived from ERA5 reanalysis data. Zonal mean Theta and wind (20,30,40m/s) contours are indicated by the magenta and grey lines, respectively.

only observations within the longitude range 60°W–40°E (i.e., Atlantic and N. Africa/Europe) are considered in Figure 6. Using all available observations, as in Figure 5, yields the same seasonal features (not shown). However, values above N. America during summer at higher altitudes (<150 hPa) are higher in the respective EQLat ranges (the same might also apply to Asia but observations are too sparse to validate that), as further determined and discussed in Section 3.2.

In DJF and MAM, the driest conditions are found in the tropical UT/LS, between around 100 and 50 hPa, with H_2O_{gas} mixing ratios of mostly 2–3.5 ppmv (Figure 5a). This well-known dry feature is also displayed in the MLS observations (Figure C1) and can be related to the annually coldest tropical cold point tropopause temperatures during that period (Fueglistaler et al., 2009). In the Northern Hemisphere sub- and extratropics (Figure 6b–d), an annual minimum is evident between 150 and 100 hPa from late winter (February) through spring. This feature persists when only considering stratospheric measurements (not shown). The tape recorder signature is also apparent, with the tropical H_2O_{gas} minimum moving to higher altitudes and latitudes over the

https://doi.org/10.5194/egusphere-2026-7153
Preprint. Discussion started: 24 November 2026
© Author(s) 2026. CC BY 4.0 License.

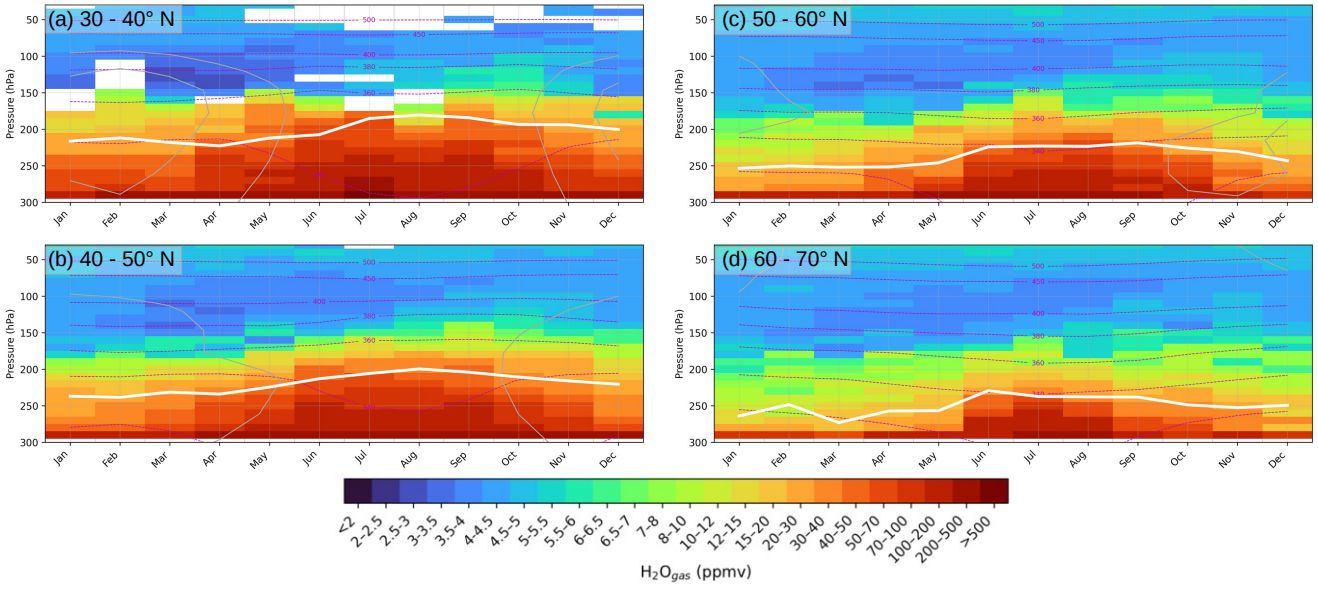

Figure 6. For the longitude range 60° W to 40° E (Atlantic and Europe/N. Africa), monthly mean H_2O_{gas} on pressure levels for different EQLat ranges from TPC&NDACC data. The white solid, magenta dashed and grey solid lines indicate the mean thermal tropopause level, and Theta and wind (20,30 m/s) contours, respectively.

following months. This likely corresponds to the ascend of the winter minimum from the tropical tropopause region to higher altitudes and the subsequent mixing of these dry air masses into the sub- and extratropics from progressively higher altitudes. Additional reasons for drier values in the extratropical LS in winter and spring are the stronger contribution of descending deep-stratospheric air masses associated with the Brewer-Dobson circulation (Appenzeller et al., 1996), originating from the tropics, as indicated by the observation of the highest O_3 values in the LS during those seasons (Figure C3). Moreover, lower cold-point temperatures during winter in the Northern Hemisphere extratropics (Hoor et al., 2010; Zahn et al., 2014) imply that the entrained extratropical tropospheric air masses there are also drier.

In the Southern Hemisphere, very dry conditions are observed in polar air masses (EQLat>60° S) in SON (Figure 5d), which can be attributed to dehydration along the polar jet during southern winter and spring (Rolf et al., 2015). These observations are based primarily on a single measurement campaign over South America (TACTS-ESMVal; Rolf et al., 2015), raising the question of how climatologically representative they are. However, observations from MLS also reveal a similar dry feature in the LS, which is evident in every year of the record (Figure C1).

During summer, a pronounced hydration of parts of the UT and LS is evident across all latitude bands in the Northern Hemisphere sub- and extratropics (Figure 6). In extratropical air masses between 50–60°N EQLat (Figure 6c), a seasonal maximum around 150 hPa and higher occurs in July. When considering only observations above the thermal tropopause, this feature persists, demonstrating that it is not confined to the UT. Over N. America, this seasonal maximum is evident up to 100 hPa (not shown), whereas over the 60°W–40°E band, the maximum occurs between September and November near

https://doi.org/10.5194/egusphere-2026-7153
Preprint. Discussion started: 24 November 2026
© Author(s) 2026. CC BY 4.0 License.

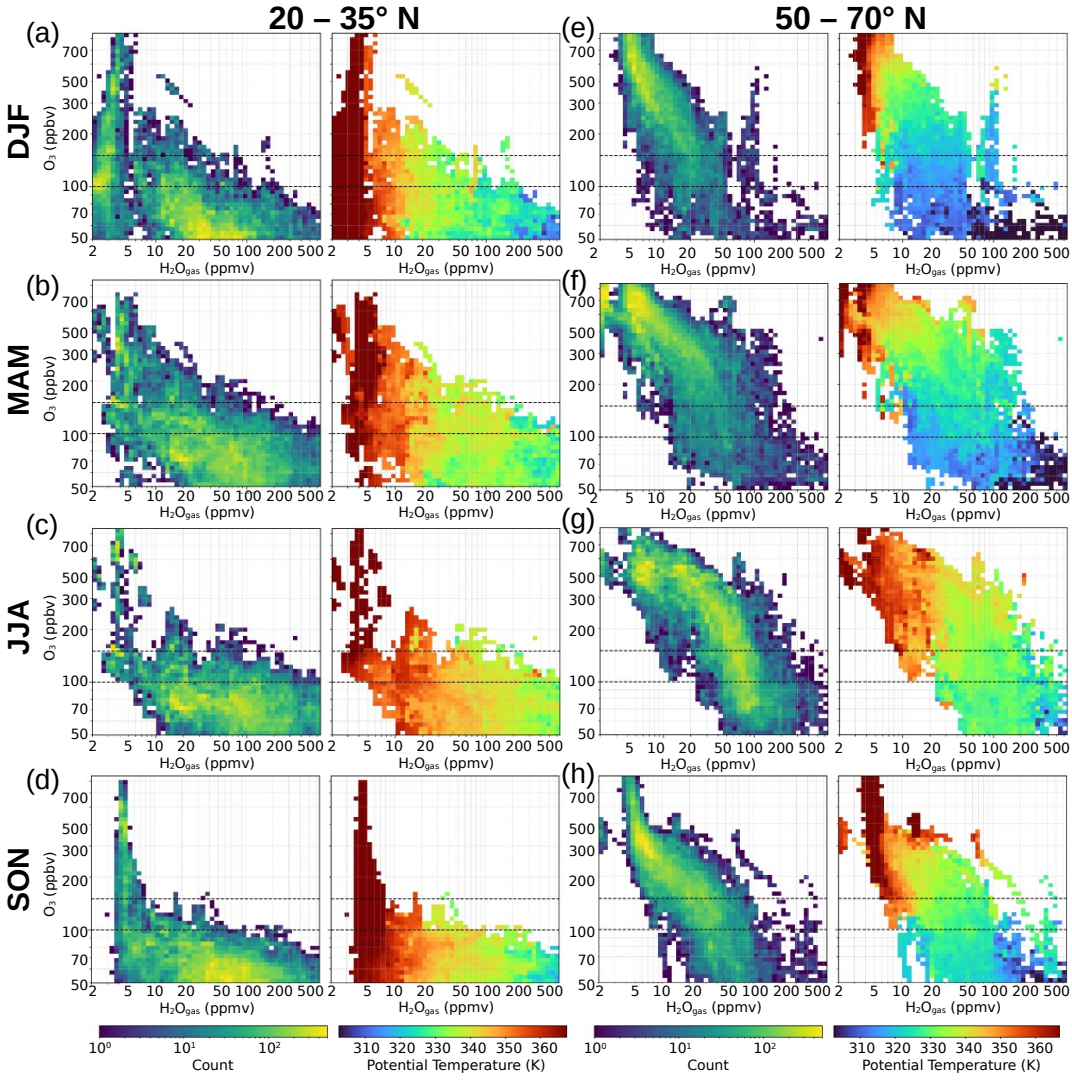

Figure 7. H_2O_{gas}-O_3 correlations from TPC. Correlations are shown for two EQLat ranges (EQLat 20-35° N in panel a-d and 50-70° N in panel e-h) and for every season. In every panel, total number of measurements (left) and mean Theta (right) are shown.

100 hPa. The maximum in fall can be explained by the contribution of the Asian monsoon circulation, which typically develops in July and begins to influence the extratropics from August onward. The delayed maximum can be attributed to the isentropic transport of moist air masses originating within the Asian monsoon anticyclone into the extratropics (Bönisch et al., 2008; Ploeger et al., 2013).

Tracer–tracer correlations between H_2O_{gas} and O_3 (Figure 7) further show that H_2O_{gas} increases relative to O_3 throughout the entire extratropical LS during summer (panel g; 50-70°N EQLat). Trajectory analyses (Hoor et al., 2010; Zahn et al., 2014)

https://doi.org/10.5194/egusphere-2026-7153
Preprint. Discussion started: 24 November 2026
© Author(s) 2026. CC BY 4.0 License.

suggest that this behavior is linked to elevated Lagrangian cold point temperatures in summer, which enhance stratospheric H_2O_{gas} and shift H_2O_{gas} in the H_2O_{gas}–O_3 correlation toward higher mixing ratios. As discussed further in Section 4, this can lead to the transport of comparatively moist air masses into the extratropical LS during summer, with H_2O_{gas} concentrations exceeding 100 ppmv at the Lagrangian cold point, in contrast to typically less than 5 ppmv at the tropical cold point tropopause. One possible interpretation is that the summertime enhancement of H_2O_{gas} in the extratropical LS is primarily driven by seasonal changes in the Lagrangian cold-point temperature, combined with enhanced isentropic mixing along the subtropical jet. During summer, the transport barrier associated with the subtropical jet is substantially weaker than in winter, facilitating increased exchange between the tropics and extratropics (Kunz et al., 2015). An additional explanation is that transport associated with deep convection in the extratropics and adjacent subtropics, followed by rapid isentropic redistribution, contributes additionally to the observed enhancement.

An important outstanding question is whether such deep convective transport is required to explain the observed summertime increase in H_2O_{gas}, or whether it can instead be accounted for solely by the higher cold-point temperatures encountered by air masses entering the LS during summer. Trajectory-based analyses are therefore needed to distinguish between these mechanisms and to quantify the relative importance of convective transport. The potential effect of convective moistening will be further investigated in Section 3.2.

3.2 The geographical variability of H_2O_{gas}

In order to determine the geographical variability, MOZAIC&CORE$_{adj}$ multi-annual monthly means of H_2O_{gas} are presented in Figure 8 (January and April) and Figure 9 (July and October). Data are shown as a function of potential temperature (Theta) rather than pressure or altitude because Theta better characterizes air mass transport in the UT/LS; owing to the nearly constant cruising altitude of passenger aircraft, different Theta levels correspond to different air masses. Levels below 340 K predominantly correspond to extratropical air around tropopause level. Higher Theta levels correspond to (sub)tropical UT and, at the higher cruising altitudes (mostly $>$11km), also to extratropical LS air masses.

In January, the highest H_2O_{gas} concentrations in the mid-latitude 325–340 K range are found over the N. Atlantic. A similar pattern is also evident in October, though slightly shifted to higher Theta levels (335–350 K). When examining pressure levels instead of Theta (not shown), a winter maximum over the Atlantic compared to continental regions at the same latitudes is also evident.

The enhanced H_2O_{gas} concentrations over the Atlantic might be related to a greater occurrence of baroclinic instability compared to the more stable continental extratropical regions during the winter half of the year (Pepler and Dowdy, 2021). In previous studies, the higher low-pressure activity over this area was found to lead to a higher frequency, compared to continental regions, of large-scale uplift of moist air masses, especially within warm conveyor belts (WCB), thereby moistening the UT (Schwenk and Miltenberger, 2024; Guo and Miltenberger, 2025). Reutter et al. (2015) showed that, over the Atlantic, mixing between the UT and the LS is enhanced during cyclonic conditions. Specifically, WCBs have been linked to enhanced isentropic transport into the LS (Kunkel et al., 2019; Guo and Miltenberger, 2025; Schwenk and Miltenberger, 2024), thereby moistening not only the UT but also potentially contributing to a moistening of the LS. A further assessment of whether the evident moister

https://doi.org/10.5194/egusphere-2026-7153
Preprint. Discussion started: 24 November 2026
© Author(s) 2026. CC BY 4.0 License.

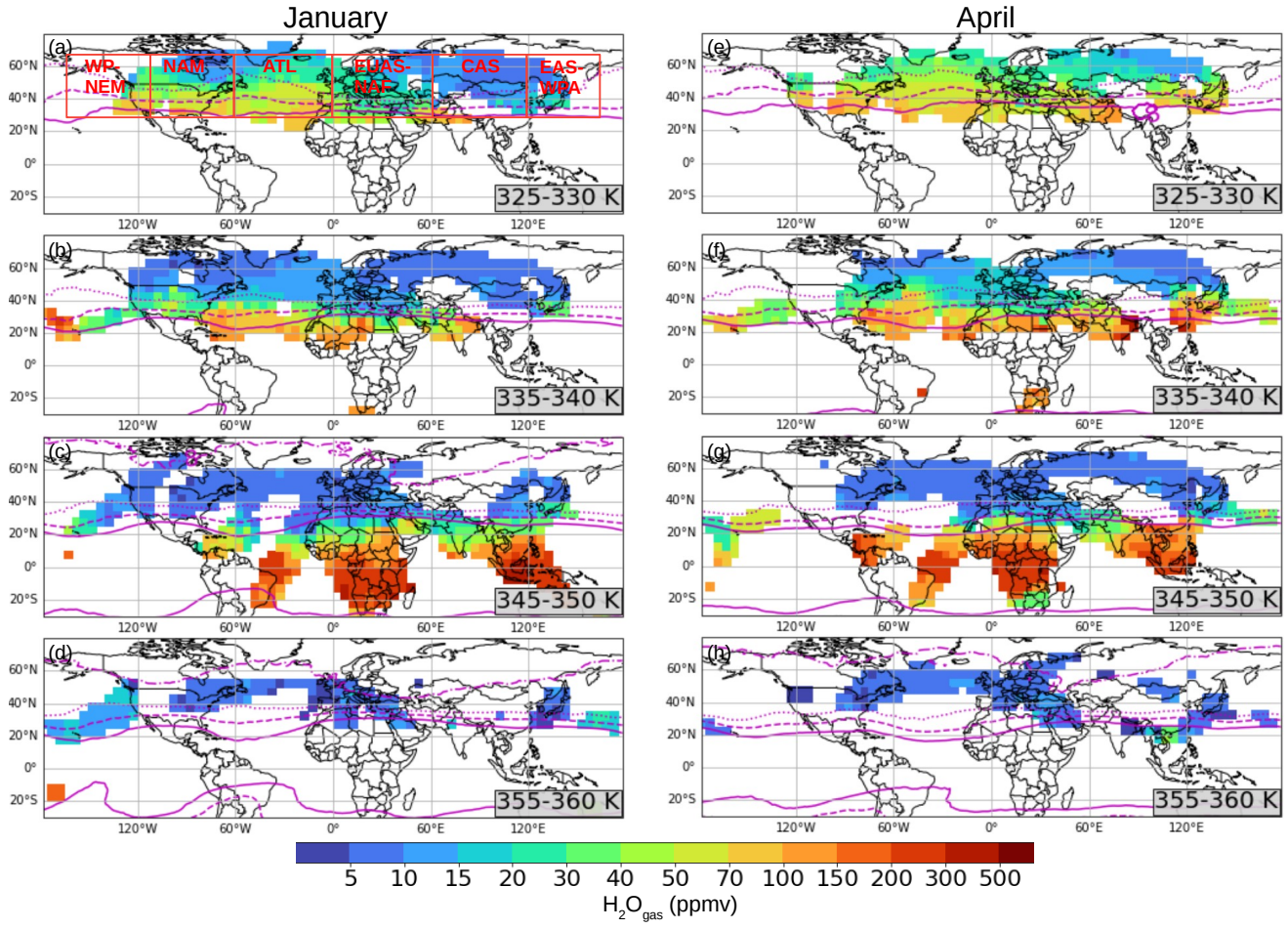

Figure 8. MOZAIC&CORE$_{adj}$ $\mathbf{H_2O_{gas}}$ **climatologies on Theta levels**. Monthly means (January and April) are shown at four Theta levels. The magenta solid, dashed, dotted, and dash-dotted lines indicate the mean position of the 2, 4, 6 and 8 PVU levels, respectively. In panel (a), the regions highlighted for further analysis in subsequent sections are marked by red boxes.

conditions over the Atlantic also extend into the LS or are related (only) to moister UT conditions is performed in Section 3.2. During July, over parts of N. America as well as S.E. Asia, the monsoon-related H_2O_{gas} increase is evident. At 345-350 K (Figure 9c), mean values are higher by a factor of 3 (N. America) to 10 (SE. Asia) compared to other regions at the same geographic latitudes. Over the Asian monsoon region, where the cold point tropopause level may even exceed 380 K (Clemens et al., 2022) compared to mostly <340 K in extratropical air masses, H_2O_{gas} concentrations exceed 300 ppmv even at 355-360 K, whereas in most extratropical regions, mixing ratios are below 10 ppmv, i.e., around or close to stratospheric background concentrations, at this level.

Building on the results presented in Figure 8 and Figure 9, a comparison for the northern subtropical and extratropical latitudes (30-70° N), where MOZAIC&CORE$_{adj}$ provides the most extensive data coverage, is presented across different sub-regions

https://doi.org/10.5194/egusphere-2026-7153
Preprint. Discussion started: 24 November 2026
© Author(s) 2026. CC BY 4.0 License.

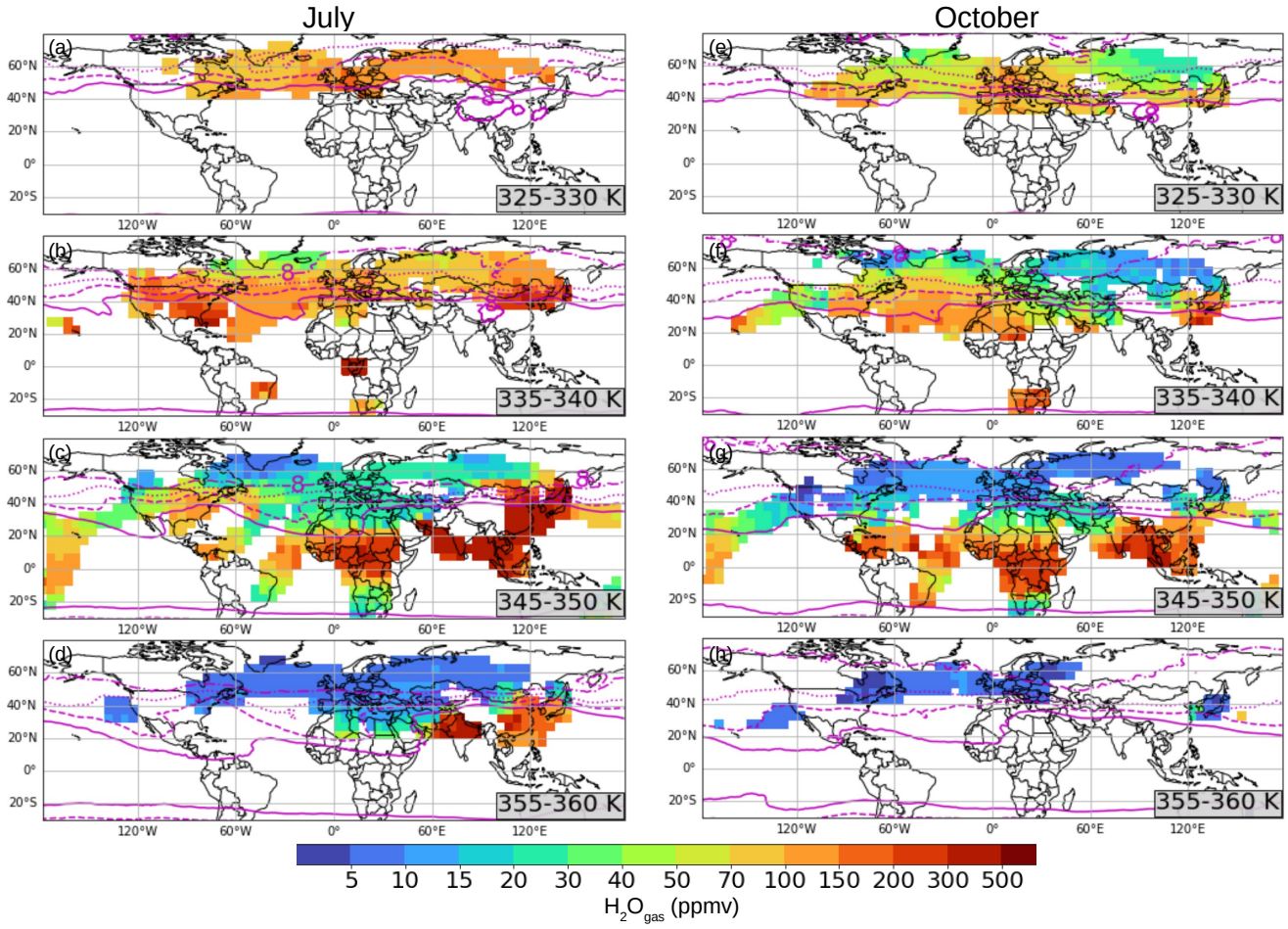

Figure 9. Same as in Figure 8 but for July and October.

defined in Figure 8a. In Figure 10, zonal mean seasonal profiles of H_2O_{gas} and O_3, as well as the corresponding mean tracer–tracer correlations, are shown for the three regions North America (NAM), Atlantic (ATL), and Central Asia (CAS). In order to determine if certain features observable in Figure 8 and Figure 9, like the moist features over the Atlantic in fall and winter, also extend into the LS, only observations corresponding to LS air masses are considered, based on filtering with the chemical tropopause O_3 (TTP_{O_3}) values derived in Zahn et al. (2004). Seasonal means are derived by averaging monthly means, and a seasonal mean is only computed if all three constituent months provide valid mean values.

Especially in DJF, but also in MAM and SON, moister conditions over the ATL at higher mid-latitudes ($> 50°N$) are evident. For O_3, a stronger tropospheric footprint over ATL is evident, while in the tracer–tracer correlations the profiles of the different regions, as well as those of the different zonal bands, lie very close to each other (especially in DJF and MAM). This points either to enhanced UT-to-LS transport and/or a higher tropopause level, rather than differences in the dehydration rates of the corresponding air masses. Consistent with this, the STE climatology in Sprenger and Wernli (2003) indicates generally weaker

https://doi.org/10.5194/egusphere-2026-7153
Preprint. Discussion started: 24 November 2026
© Author(s) 2026. CC BY 4.0 License.

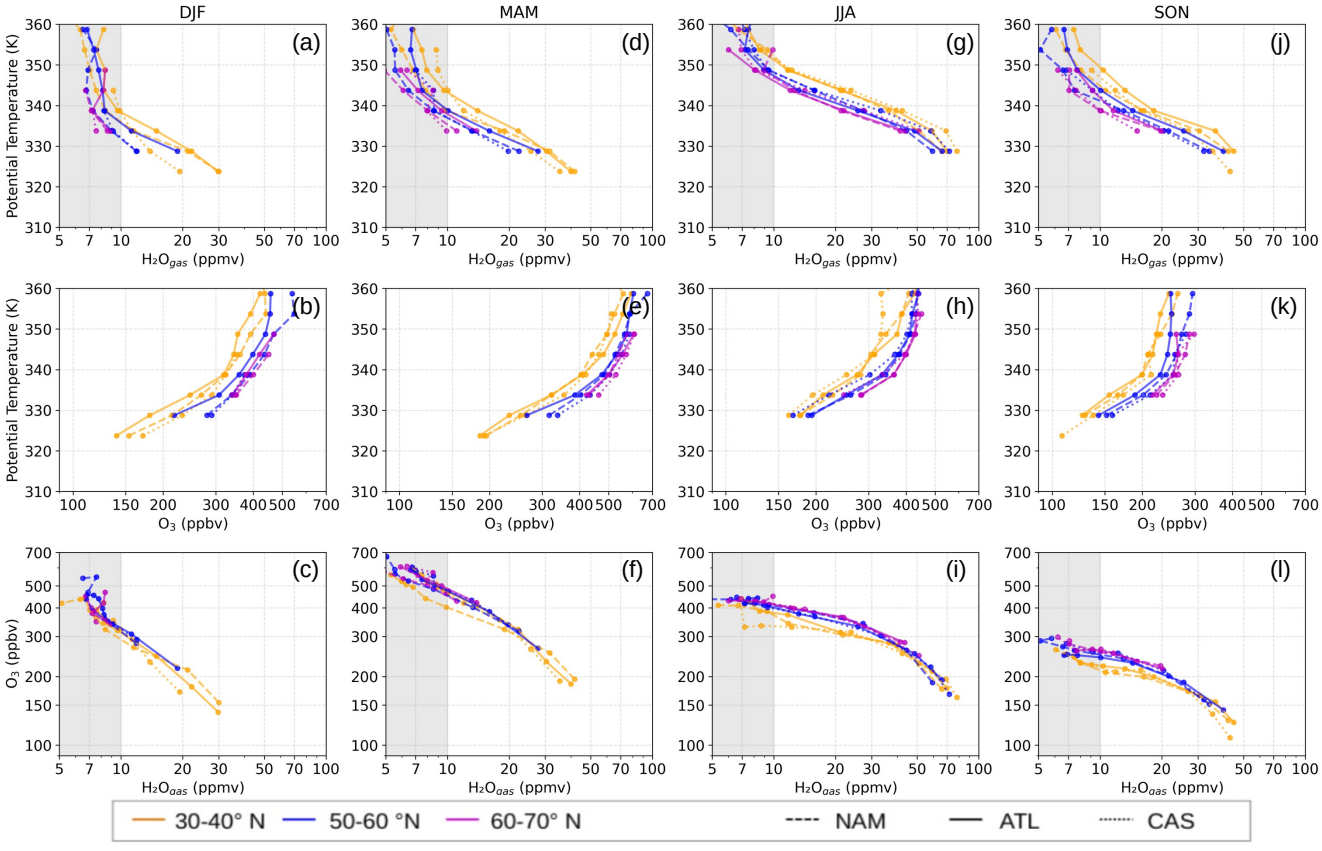

Figure 10. IAGOS-MOZAIC&CORE adjusted H_2O_{gas} and O_3 profiles, and the corresponding tracer-tracer correlations, for the different seasons and latitude ranges for the three regions N. America (NAM), Atlantic (ATL) and C. Asia (CAS). Only data above the chemical O_3 tropopause are taken into account. The grey dashed area represents the H_2O_{gas} range where uncertainties increase to more than around 20 %.

mixing over continental Asia compared with the Atlantic at the same latitude. Furthermore, these LS Theta levels are situated, on average, higher above the tropopause over both continental regions than the corresponding bins over ATL, as evident from ERA5 tropopause data (not shown).

In JJA, the regional differences are smaller, compared to the other seasons, within the respective latitude ranges, and the overall gradient between the latitude ranges is also weaker. Compared to ATL, moister features over CAS are evident along all three latitude bands, while over NAM they are evident in the 50–60°N latitude band. In O_3, a stronger tropospheric footprint, i.e., lower O_3 mixing ratios, is evident over CAS and NAM for the 30-40°N latitude range in JJA, especially over CAS but also over NAM. This stronger tropospheric footprint, however, correlates with drier air masses in the tracer-tracer correlations, i.e. potentially more strongly dehydrated air masses of more tropical origin.

In order to further disentangle regional differences, and specifically to investigate potential regional differences related to turbulent, i.e. diabatic, mixing processes such as convection, Figure 11 shows seasonal mean profiles of H_2O_{gas} and O_3 for

https://doi.org/10.5194/egusphere-2026-7153
Preprint. Discussion started: 24 November 2026
© Author(s) 2026. CC BY 4.0 License.

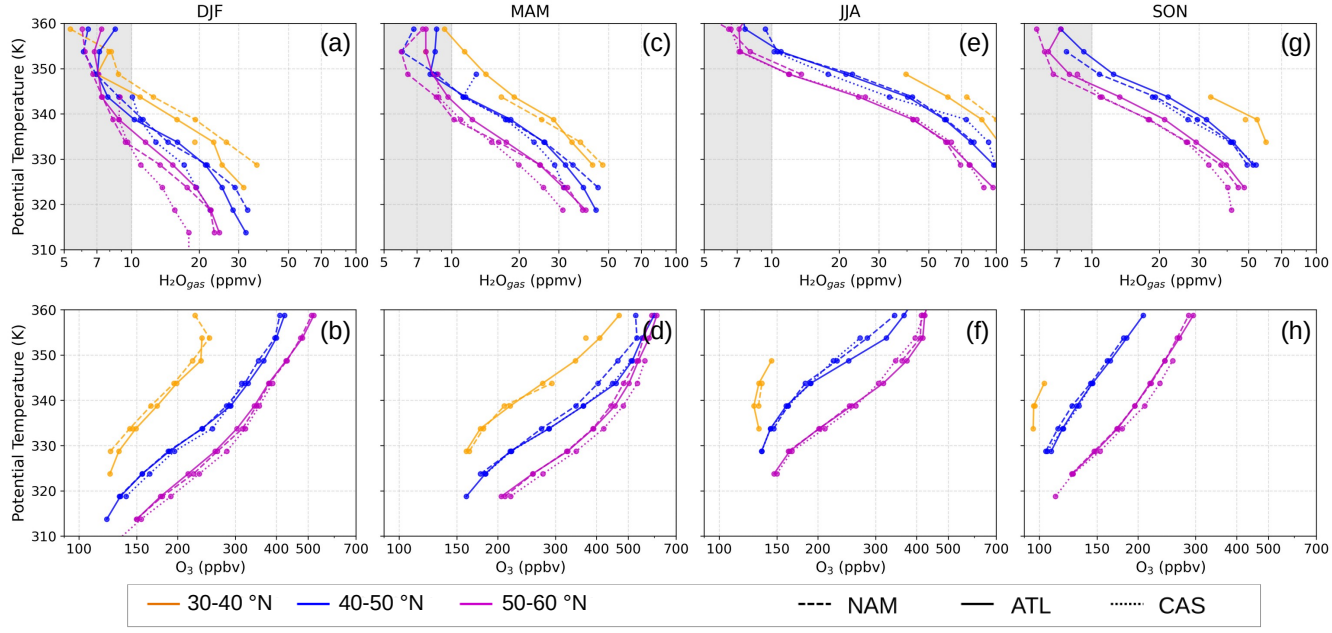

Figure 11. IAGOS-MOZAIC&CORE adjusted H_2O_{gas} (upper row) and O_3 (lower row) profiles for the different seasons, as in Figure 10 but for EQLat instead of latitude ranges, for NAM, ATL and CAS.

EQLat instead of latitude ranges, using all data from the defined regions (i.e., over 30-70°N). Additionally, in Figure C4 (NAM, EUAS-NAF, CAS) and Figure C5 (EAS-WPA, EPA-NEAM), the corresponding sampling mean H_2O_{gas} (monthly means and 5K-5° Theta-EQLat ranges) of the regions are scattered against ATL as reference.

Generally, from an EQLat perspective, the differences between the EQLat ranges are much larger than those observed from a latitude perspective, clearly showing that EQLat accounts for reversible excursions of the tropopause by planetary waves. It therefore accounts for the tracer gradients relative to the tropopause in isentropic direction and thus separates the mean mixing ratios as a function of horizontal distance (and thus transport time) from the tropopause (e.g., Hoor et al., 2010). Considering regional differences, Figure 11 reveals that from fall to spring, in the 50–60°N and 60–70°N EQLat ranges, air masses over ATL remain moister compared to the CAS and NAM (only in the 60–70°N EQLat range) below around 330–340 K. In contrast, there is no clear signal in O_3 that would indicate substantially reduced UT-to-LS mixing at these levels, although O_3 values are also slightly elevated over CAS which points toward stronger dehydration processes as the main reason for the drier conditions. Interestingly, in DJF, higher H_2O_{gas} mixing ratios are found over NAM in the 30–40°N EQLat range. For O_3, lower values indicate enhanced UT-to-LS mixing, although the differences are less pronounced than those observed for H_2O_{gas}. This could be explained by convective moistening. In winter, substantial convection is already occurring over NAM (Pettegrew et al., 2009), and during this season the tropopause is also lower, such that passenger aircraft are more likely to sample its impact. In contrast, in summer, when such overshooting convection occurs mostly under higher tropopause conditions, the air masses may already be more zonally homogenized by the time they reach more extratropical levels, such that regional differences are

https://doi.org/10.5194/egusphere-2026-7153
Preprint. Discussion started: 24 November 2026
© Author(s) 2026. CC BY 4.0 License.

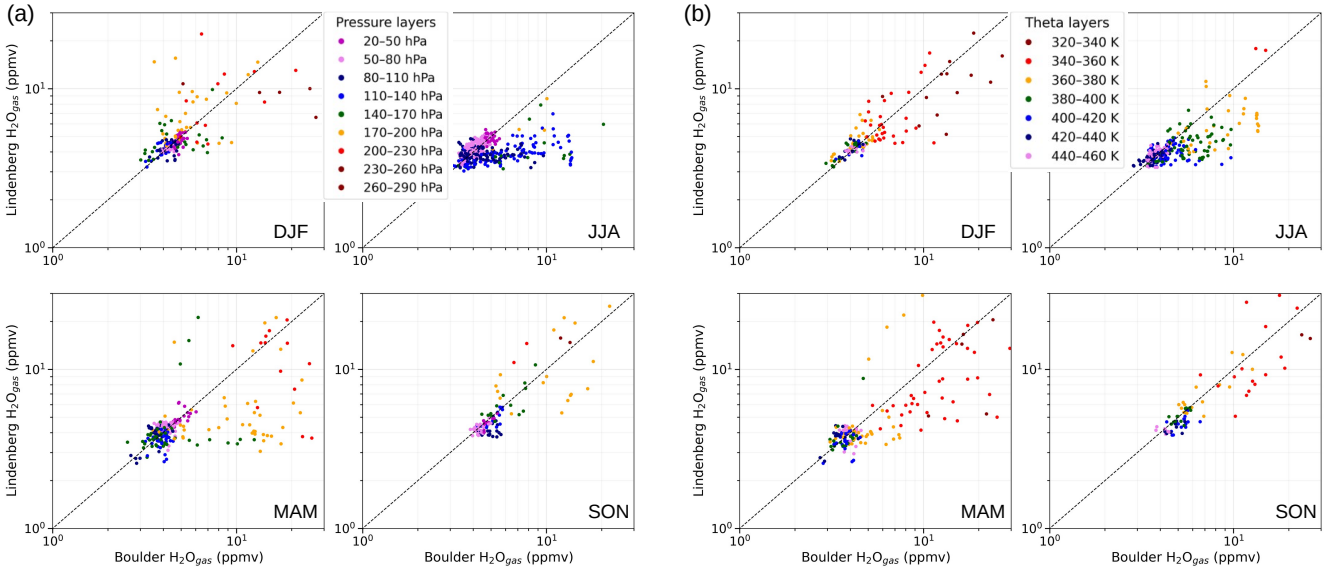

Figure 12. Intercomparison of NDACC frost point hygrometer observations over Boulder and Lindenberg. Data are sampled into different years and months, and then into EQLat and pressure (a) or Theta (b) ranges. For every season, all corresponding matches are scattered against each other. Only measurements above the thermal tropopause are taken into account.

no longer detectable. This might explain why, in JJA, no moist features are observed over the continental regions compared to ATL. An exception is found at lower Theta levels, although this could be related to uncertainties in distinguishing between UT and LS air masses based on O_3 values, i.e., UT air masses might account for the moister conditions observed in the figure.

At altitudes higher than those typically sampled by passenger aircraft, however, satellite observations consistently reveal moister conditions during summer over the monsoon regions over N. America and Asia (e.g., MLS and SAGE-III; Wang et al., 2025). To assess whether this feature is also evident in balloon-borne observations, data from the two stations at Lindenberg (Germany) and Boulder (Colorado, USA) are compared. The TPC data are excluded from this intercomparison because their targeted sampling of convective events, particularly during campaigns in the United States, could bias the comparison. Furthermore, the TPC observations are too sparse, except over Europe, to support a robust intercomparison.

In order to compare the data, they were sampled into EQLat to account for the different synoptic conditions determining the tropopause location, and into pressure or Theta ranges. From this sampling, monthly means are calculated for all years separately (i.e., as shown in Figure C2). The corresponding means are then scattered against each other, as shown in Figure 12. In both pressure (a) and Theta (b) coordinates, moister conditions are evident in MAM in the 150-230 hPa and 340-380 K range, respectively, while in DJF a slight moist bias is evident only in Theta coordinates in the 320-340 K range. In JJA, the differences become more pronounced and shift to higher levels (pressure: 80–170 hPa and Theta: 360–420 K), while above no differences are evident. This would be consistent with overshooting observed during the DCOTTS campaign reaching up to 460 K (Homeyer et al., 2023). However, this event was observed over the Midwest of the USA. Furthermore, even if similar

https://doi.org/10.5194/egusphere-2026-7153
Preprint. Discussion started: 24 November 2026
© Author(s) 2026. CC BY 4.0 License.

events also occur over and near Boulder, or are transported there, it remains unclear whether they contribute significantly to the overall climatological moistening.

In general, the differences are stronger in pressure than in Theta coordinates. This indicates that differences in Theta and the corresponding pressure levels between Boulder and Lindenberg contribute to the larger biases. However, using Theta as a transport-relevant coordinate reduces these biases.

In DJF and MAM, there is a tendency towards moister conditions over Boulder, including at passenger aircraft cruising altitudes. According to the IAGOS-MOZAIC&CORE climatology (Figure 11), conditions are also moister in DJF (30–40°N EQLat) over N. America compared to North Atlantic (which shows similar mean profiles to Europe; see Figure C4). However, there is no moist feature over N. America evident in spring, in contrast to Lindenberg vs Boulder. Nevertheless, the use of broad geographical regions instead of fixed locations might smooth out local moist features. Furthermore, the differences in MAM occur predominantly at low mixing ratios ($<$10 ppmv), where the relatively large bias of the IAGOS-MOZAIC&CORE profiles could outweigh potential differences.

Owing to its relatively southern location (40°N), no stratospheric air at pressure levels greater than 200 hPa was sampled over Boulder during any of the JJA balloon soundings. Consequently, it cannot be determined from these observations whether convection associated with the N. America monsoon also moistens those higher layers locally.

4 Discussion and conclusion

Using an extensive set of available in-situ datasets, ipassenger aircraft, research aircraft, and balloon-borne measurements, the seasonal and geographical variability of H_2O_{gas} was examined. Pronounced moist features were found to occur over the Atlantic from fall through spring, where moister conditions are evident for extratropical LS air masses with Theta $<$ 340 K. Several studies (Kunkel et al., 2019; Guo and Miltenberger, 2025; Schwenk and Miltenberger, 2024) found that, in connection with the outflow of WCBs, the uplifted air masses experience enhanced isentropic mixing into the LS. Furthermore, frontal systems are associated with enhanced turbulent STE driven by wind shear and gravity wave breaking, thereby transporting moist UT air masses into the LS. The observed overall moister conditions over the extratropical Atlantic support the hypothesis that mixing associated with cyclonic activity leads to enhanced moistening of the exTL also from a statistical point of view. The Atlantic region could therefore represent an important gateway for H_2O_{gas} and other tracers from the UT into the exTL. The same might also apply to the North Pacific and the Southern Hemisphere oceanic regions where high low-pressure activity is evident (Akritidis et al., 2016). However, there are too few IAGOS data over those areas to further validate this hypothesis.

From the adjusted MOZAIC&CORE climatologies, there is only weak evidence of convective moistening of the sampled extratropical LS air masses, at least not at passenger aircraft altitude, although signatures are observable in the UT, particularly over N. America and Asia. One potential reason could be that passenger aircraft avoid heavy convective systems, thereby not sampling such cases in their early stages when convection is still active. Furthermore, LS air masses observed by passenger aircraft have tropopause heights below 12 km, as the stacked flight altitudes rarely exceed 12 km and are usually below 11 km. Consequently, sampled LS air masses are of extratropical origin with relatively low tropopause levels, which exhibit reduced

https://doi.org/10.5194/egusphere-2026-7153
Preprint. Discussion started: 24 November 2026
© Author(s) 2026. CC BY 4.0 License.

convective instability, limiting the likelihood of directly sampling convectively influenced air. Most cases described in previous studies (e.g., Homeyer et al., 2024; Khordakova et al., 2022) are typically associated with convection in more subtropical air masses and, consequently, with higher tropopause levels exceeding 12 km. An overshooting case observed during the TPEx (TropoPause compositon gradients and mixing Experiment; Bozem et al., 2025) campaign, however, associated with a tropopause height of only 9 km (Konjari et al., 2025b), demonstrates that such events do occur in the extratropics and can be linked to enhanced LS H_2O_{gas}, although their overall frequency remains uncertain. From the balloon soundings over Boulder, there is an indication of elevated H_2O_{gas} also in LS air masses at passenger aircraft altitude in spring. As for passenger aircraft, those soundings do not sample fresh convection, thereby the argument that it is not visible because it wasn't sampled directly in the early state is not valid.

The NDACC frost point hygrometer observations over Boulder show, compared to observations over Lindenberg, strong enhancements of H_2O_{gas} especially in the layers above passenger aircraft altitude, around or close to stratospheric background level around 380 K, during spring and summer (in 140-200 hPa and 80-170 hPa, respectively), in agreement with enhancements also evident from satellite observations. Based on MLS observations, Jensen et al. (2024) demonstrated that, globally, the strongest H_2O_{gas} outliers in the LS at around 100 hPa can be found over N. America.

Overall, it remains unclear how the overall zonal influence of such convection, after rapid zonal transport on timescales of sometimes only a few days, contributes to the observed summer moistening of the LS in the extratropics. More generally, in the extratropics at higher latitudes, relatively high tropopause temperatures can also allow the transport of very moist air into the LS, which contributes to a seasonal maximum in H_2O_{gas} below 360 K in the extratropics. In the tracer-tracer correlations shown in Figure 7, the highest mixing ratios observed in summer in the extratropical LS come from both overshooting convection cases (e.g., during CIRRUS-HL [Cirrus in High-Latitudes; (Jurkat-Witschas et al., 2025)] and TPEx [TropoPause composition gradients and mixing Experiment; (Konjari et al., 2025b)]) but also from non-convective flights. A tropopause folding event observed during TPEx in particular highlights that non-convective turbulent mixing processes, indicated by the presence of cloud particles in subsaturated air with O_3 values up to 300 ppbv, can lead to very high H_2O_{gas} mixing ratios exceeding 100 ppmv (Emig et al., 2026). However, compared to the overshoot cases during CIRRUS-HL and TPEx, Theta values are much lower (e.g., 300 ppmv H_2O_{gas} at around 200 ppbv O_3 and 320 K Theta).

This indicates that possibly, in the lower layers of the extratropical LS, non-convective mixing is likely a dominant contributor to a seasonal summer peak by a considerable margin. At higher potential temperatures (approximately 340 K and above), convective transport may become increasingly important. However, the relative contributions of these processes in the upper layers remain uncertain.

Overall, this study enhances our understanding of the H_2O_{gas} variability and provides quantitative constraints on mixing ratios, which remain uncertain in both model simulations and satellite observations. It therefore highlights the importance of jointly analyzing the available in-situ observations to obtain a more comprehensive picture. An important direction for future research is to better quantify the regional radiative effects of H_2O_{gas} from those in-situ observations to improve our understanding of the role of UT/LS water vapor in the climate system.

https://doi.org/10.5194/egusphere-2026-7153
Preprint. Discussion started: 24 November 2026
© Author(s) 2026. CC BY 4.0 License.

. Acknowledgements. Parts of the study were funded by the Deutsche Forschungsgemeinschaft (DFG, German Research Foundation) – TRR 301 – Project-ID 428312742. Parts of the study were also funded by ESA (contract no. 4000123554) via the Water Vapour Climate Change Initiative (WV_cci) project phase 2 of ESA's Climate Change Initiative (CCI).

This research was supported by the International Space Science Institute (ISSI) in Bern, through ISSI International Team project 24-620 (Climate Impacts of Stratospheric Water Vapour), as well as by the Observed Composition Trends and Variability in the UTLS (OCTAV-UTLS) Atmospheric Processes and Their Role in Climate (APARC) activity.

The generation of the TPChange dataset was funded by the Deutsche Forschungsgemeinschaft (DFG, German Research Foundation) – TRR 301 – Project-ID 428312742. We acknowledge the European Centre for Medium-Range Weather Forecasts (ECMWF) for their ERA5 meteorological data. MOZAIC/CARIBIC/IAGOS data were created with support from the European Commission, national agencies in Germany (BMBF), France (MESR), and the UK (NERC), and the IAGOS member institutions (http://www.iagos.org/partners, last access: 12.11.2026). The participating airlines (Lufthansa, Air France, Austrian, China Airlines, Hawaiian Airlines, Air Canada, Iberia, Eurowings Discover, Cathay Pacific, Air Namibia, Sabena) supported IAGOS by carrying the measurement equipment free of charge since 1994. The data are available at https://iagos.aeris-data.fr thanks to additional support from AERIS. The frost point hygrometer data used in this publication were obtained from "NDACC PI name" as part of the Network for the Detection of Atmospheric Composition Change (NDACC) and are available through NDACC website.

. Data availability. The adjusted IAGOS-MOZAIC&CORE climatologies are available at the Zenodo platform (https://zenodo.org/records/14681370; last access: 12.11.2026). The TPChange data are available at the Zenodo platform (https://zenodo.org/records/15076520; last access: 12.11.2026). Aura Microwave Limb Sounder (MLS) version 6.0x Level 2 data were obtained from the NASA Goddard Earth Sciences Data and Information Services Center (GES DISC) at https://disc.gsfc.nasa.gov/ (last access: 12.11.2026). The ERA5 reanalysis data (Hersbach et al., 2020) were downloaded from the Copernicus Climate Change Service (C3S) Climate Data Store at copernicus.eu (last access: 12.11.2026). The Network for the Detection of Atmospheric Composition Change (NDACC; De Mazière et al., 2018) data used in this study are publicly available through the NDACC Data Host Facility (DHF), hosted at the NASA Langley Research Center (LaRC), at https://www-air.larc.nasa.gov/missions/ndacc/data.html (last access: 12.11.2026).

. Author contributions: PK analysed the data and wrote the manuscript. CR and PauK contributed to the analysis of the different in-situ datasets. HCL and PH provided the TPC and NDACC data and contributed to their analysis. HB and AZ provided the IAGOS-CARIBIC dataset and contributed to its analysis. AP and SR provided the IAGOS-CORE dataset and contributed to its analysis.

. Competing interests. At least one of the (co-)authors is a member of the editorial board of Atmospheric Chemistry and Physics. The authors have no other competing interests to declare.

Financial support. The article processing charges for this open-access publication were covered by a Research Centre of the Helmholtz Association.

https://doi.org/10.5194/egusphere-2026-7153
Preprint. Discussion started: 24 November 2026
© Author(s) 2026. CC BY 4.0 License.

Appendix A: Testing the effect of temporal inhomogeneity in the sampling of IAGOS-MOZAIC&CORE

To test the effect of the inhomogeneous coverage between the regions defined in Section 2.3.1, the Atlantic (ATL) is defined as a reference region, and the relative sampling is balanced for each year, month, and Theta-EQLat bin. For a given year and month t, let x_t denote the fraction of observations in the ATL region and y_t the corresponding fraction in a comparison region. The ratio

$$r_t = \frac{x_t}{y_t}$$

quantifies the relative sampling between the two regions.

If $r_t > 1$, the ATL region is over-represented. In this case, observations from the comparison region are randomly resampled with replacement such that their effective sample size is increased by a factor r_t. Conversely, if $r_t < 1$, the ATL observations are resampled analogously. This procedure ensures that, for each year and grid cell, both regions contribute with equal relative weight to the multi-annual statistics, and allowing for a more robust comparison of regional differences that is not driven by temporal sampling variability.

For each realization $k = 1, \ldots, m$, a resampled dataset

$$x^{(k)} = \left(x_1^{(k)}, x_2^{(k)}\right)$$

is generated, where x_1 is the original data and x_2 randomly chosen data according to the resampling scheme described above. From each resampled dataset, a multi-annual monthly mean $\bar{x}^{(k)}$ in a given bin (e.g., Theta or EQLat bin) is computed: Finally, the robust mean is obtained by averaging over all m resampling realizations:

$$\bar{x}_{\text{final}} = \frac{1}{m} \sum_{k=1}^{m} \bar{x}^{(k)}.$$

https://doi.org/10.5194/egusphere-2026-7153
Preprint. Discussion started: 24 November 2026
© Author(s) 2026. CC BY 4.0 License.

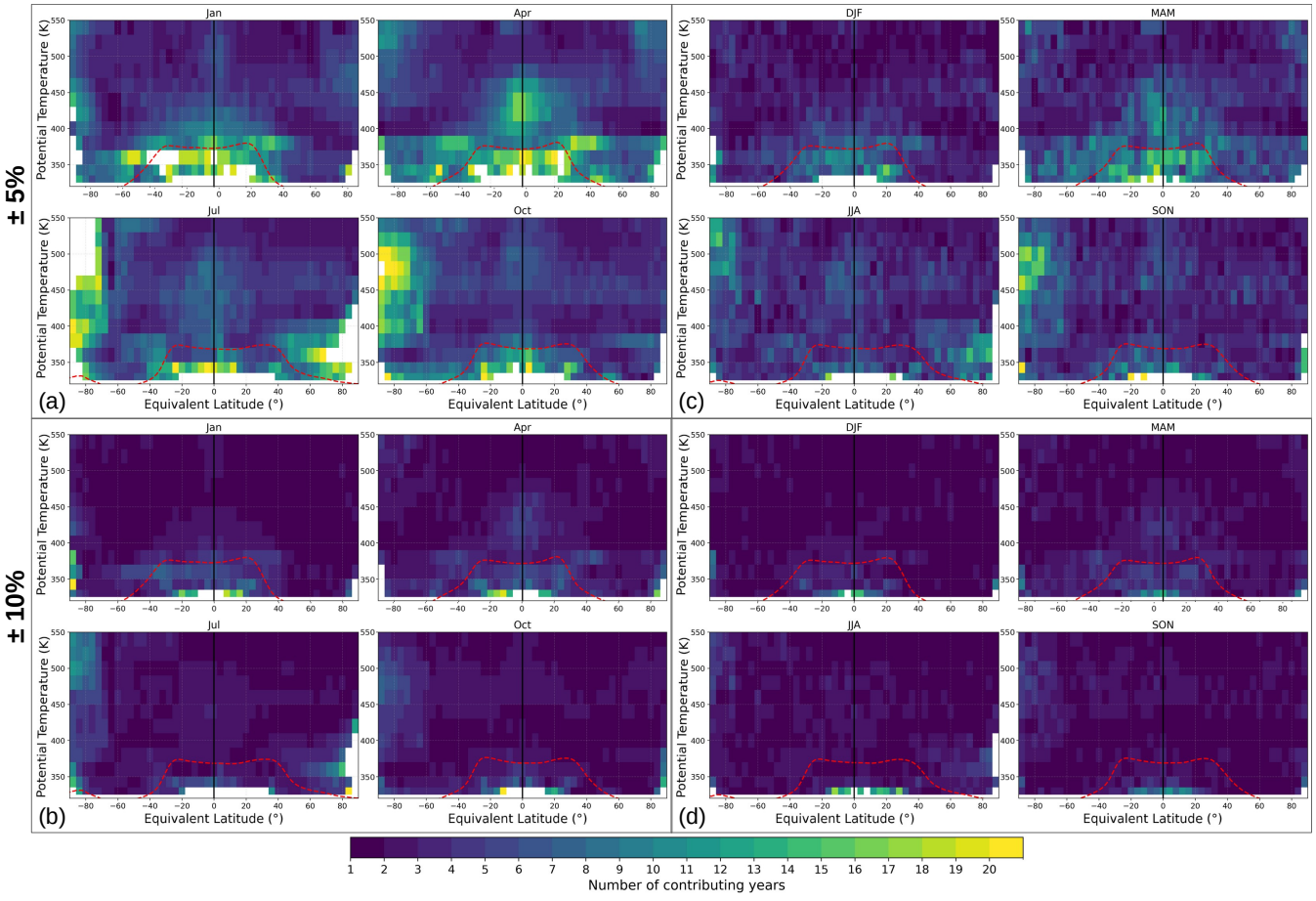

Figure B1. Bootstrap test. Based on monthly mean MLS data, the minimum number of years needed for providing, with 90% confidence, a multi-annual (here 2005-2024) mean within two uncertainty ranges (5 and 10%). Panels a&b show the results for monthly, and c&d for seasonal data.

Appendix B: Evaluation of the robustness of the TPC&NDACC based climatologies

A key question is how many TPC&NDACC observations are required to derive a meaningful climatological mean. The underlying assumption is that variability in the higher layers of the stratospheric background atmosphere is relatively small and primarily controlled by large-scale transport processes. Consequently, after sorting the observations into air-mass classes using Theta and EQLat, the remaining variability within a given month and year is expected to be limited. Under this assumption, even a comparatively small number of in-situ observations within a specific Theta–EQLat bin may be representative of the monthly mean state.

To assess this assumption, monthly means from MLS were used as a reference data set. A bootstrap analysis was performed to determine how many years of observations are required to estimate multi-annual climatological means with a specified level

https://doi.org/10.5194/egusphere-2026-7153
Preprint. Discussion started: 24 November 2026
© Author(s) 2026. CC BY 4.0 License.

of confidence. The analysis was conducted for both monthly and seasonal means. For the seasonal means, it was assumed that observations are available for all months belonging to the respective season within a given Theta–EQLat bin.

The results are presented in Figure B1. The figure shows the number of years required to estimate monthly means (a&b) and seasonal means (c&d) with 90 % confidence and relative uncertainties below 5 % and 10 %, respectively. Regions characterized by pronounced inter-annual variability clearly stand out. These include the TTL and the region extending upward to approximately 450 K, as well as the Southern Hemisphere polar jet region.

For example, in April, tropical air masses between 400 and 450 K require more than 15 years of observations to derive a climatological mean with an uncertainty below 5 %. In contrast, only about 3–5 years are required to achieve an uncertainty below 10 %. In the Northern Hemisphere extratropics above 400 K, the inter-annual variability is substantially lower, and robust climatological means can typically be obtained from only 1–2 years of observations when a 10 % uncertainty threshold is applied, both for monthly and seasonal averages. Because the JULIA data set provides coverage in a substantial number of Theta–EQLat bins within the 400–450 K layer over a period that meets or exceeds the number of years required to achieve a 10 % uncertainty threshold (Figure B1), these observations already provide valuable insight into the climatological state of this region. The corresponding Theta-EQLat grid points are highlighted in Figure 6.

https://doi.org/10.5194/egusphere-2026-7153
Preprint. Discussion started: 24 November 2026
© Author(s) 2026. CC BY 4.0 License.

Appendix C: Additional figures

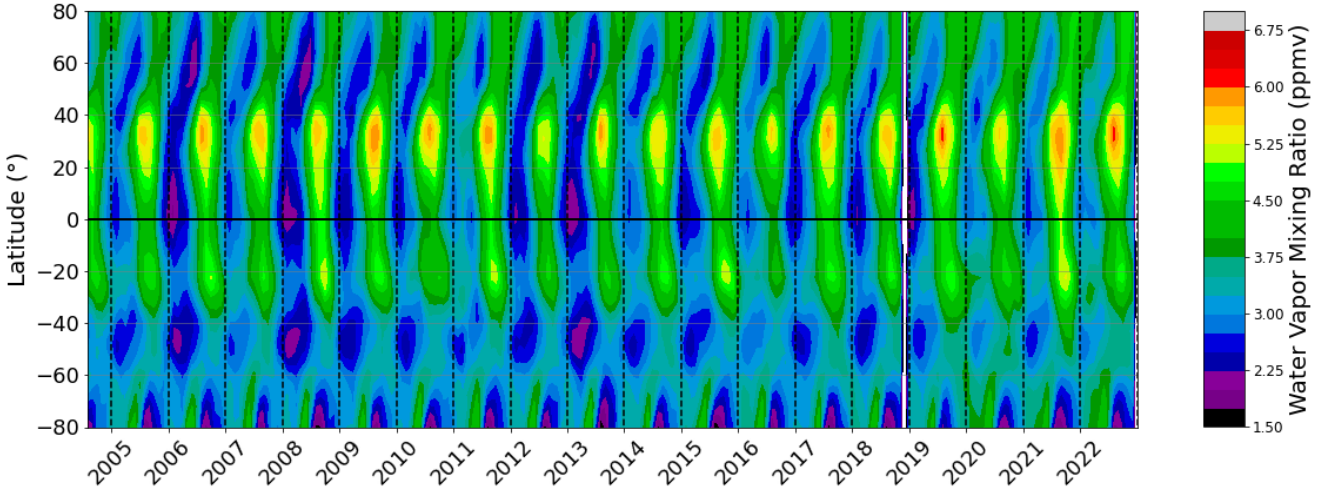

Figure C1. MLS tape recorder at 380 K.

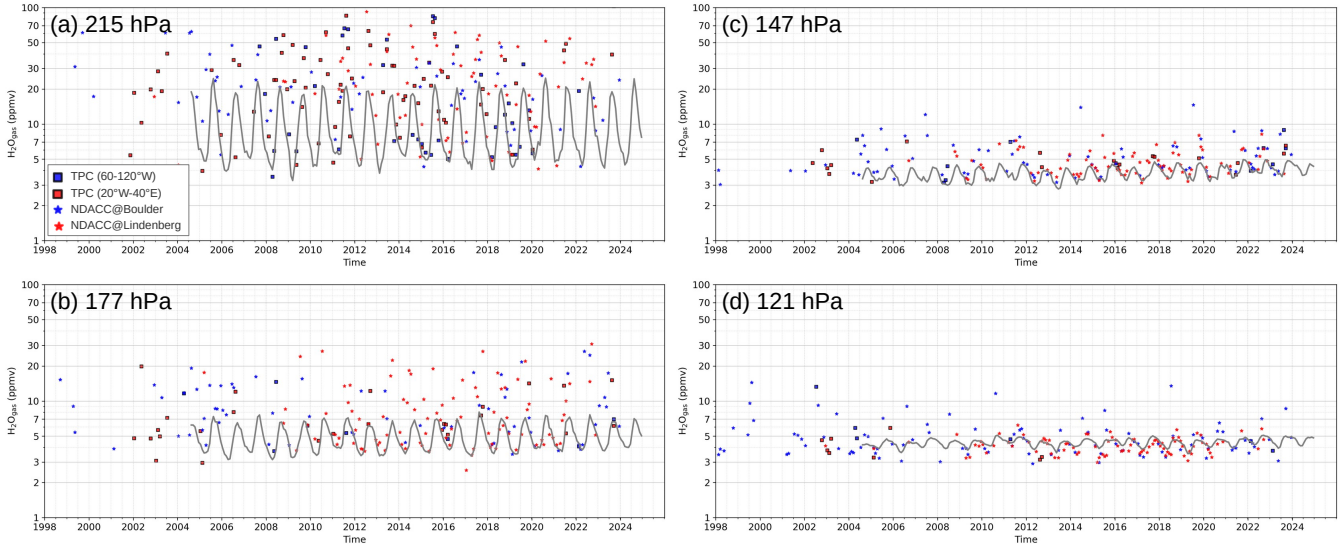

Figure C2. For different pressure levels, time series from satellite (MLS; grey line) and in-situ observations are shown. For the in-situ data, frost point observations over Boulder and Lindenberg, as well as TPC observations from two longitudinal bands (N. America and Europe/N. Africa), are shown. For both the satellite and in-situ data, only observations sampled within the 50–55°N EQLat range are utilized.

https://doi.org/10.5194/egusphere-2026-7153
Preprint. Discussion started: 24 November 2026
© Author(s) 2026. CC BY 4.0 License.

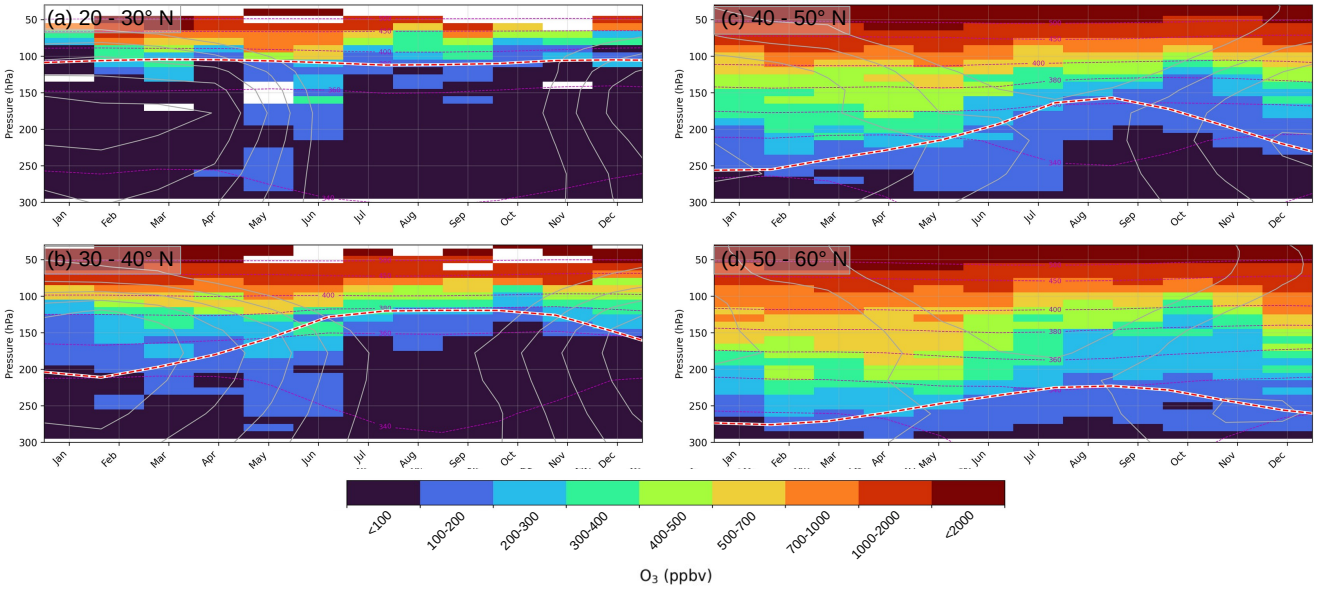

Figure C3. Monthly mean O_3 on pressure levels for different EQLat ranges from TPC&NDACC observations. Magenta and grey lines indicate potential temperature and wind contours, respectively. The mean thermal tropopause level is indicated by the red dashed line.

https://doi.org/10.5194/egusphere-2026-7153
Preprint. Discussion started: 24 November 2026
© Author(s) 2026. CC BY 4.0 License.

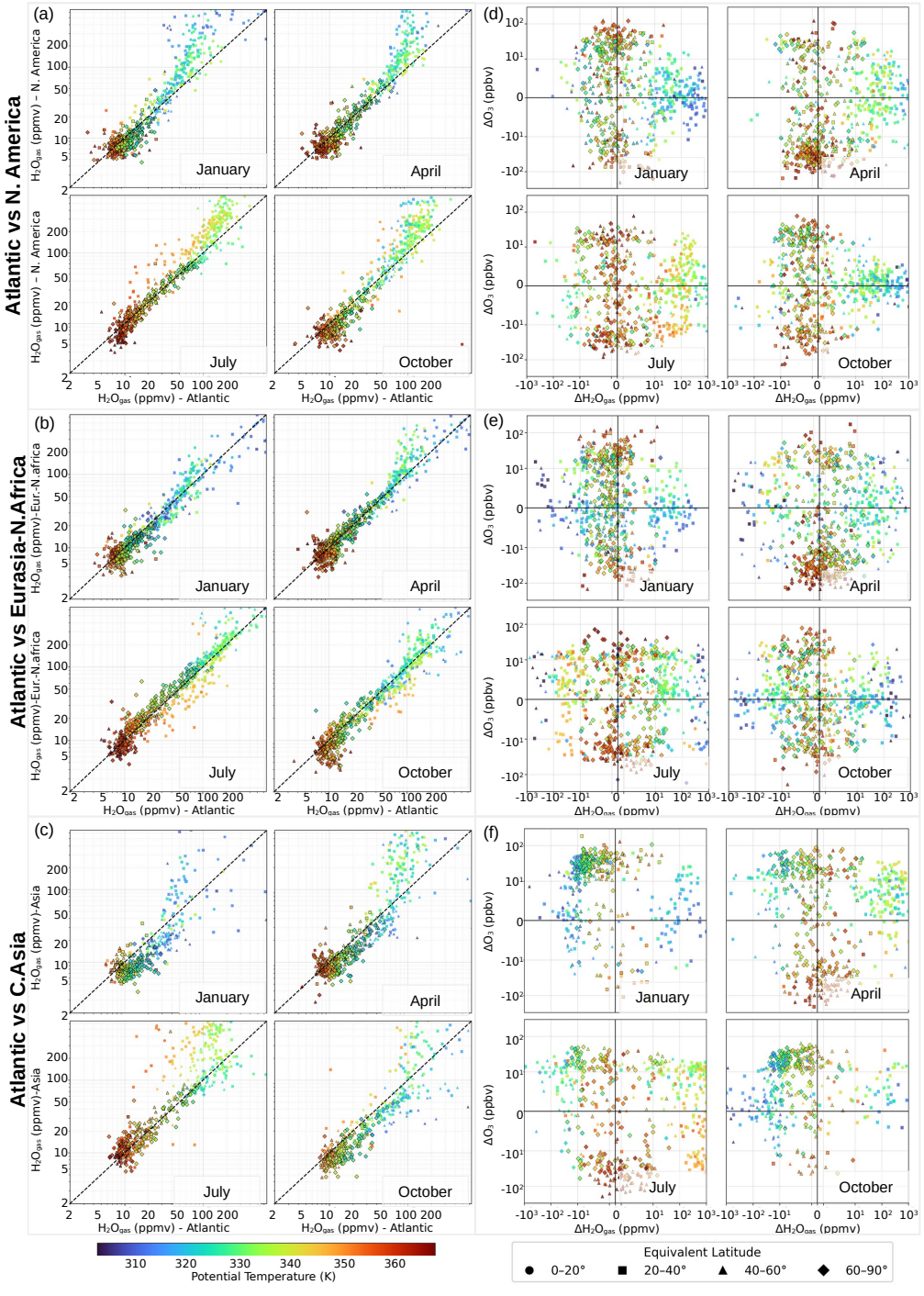

Figure C4. Intercomparison of different regions in the northern mid-latitudes. For four defined regions, N. America, Atlantic, Eurasia-N.Africa and Asia-Pacific, bin mean values of Adjusted water vapor ($H_2O_{gas,adj}$) are derived in Theta-EQLat space. In (a-c), the comparison of the corresponding mean values between Atlantic (reference) and the other regions is shown. (d-f) as in (a-c), but for $\Delta H_2O_{gas,adj}$ (x-axis) and ΔO_3 (y-axis) (Δ = Region - Atlantic).

https://doi.org/10.5194/egusphere-2026-7153
Preprint. Discussion started: 24 November 2026
© Author(s) 2026. CC BY 4.0 License.

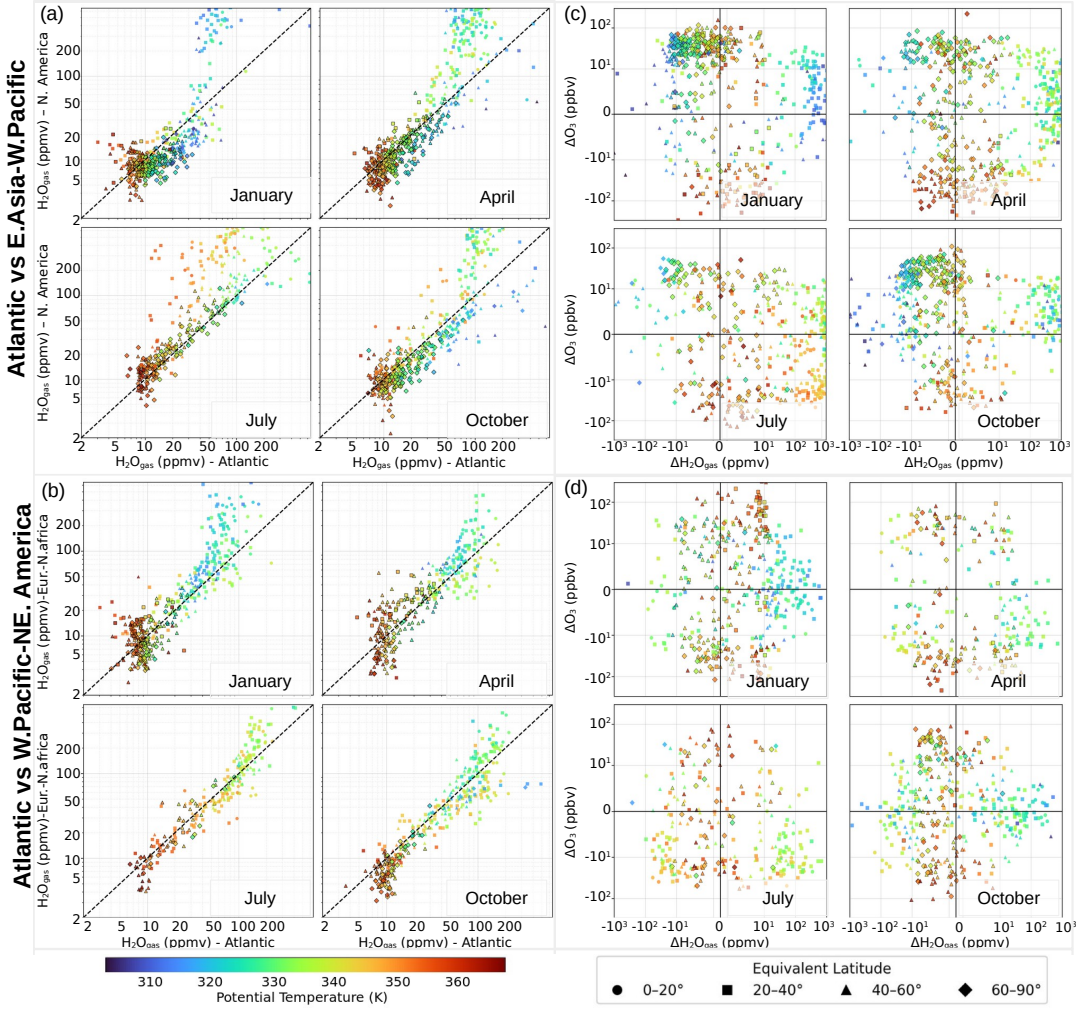

Figure C5. Intercomparison of different regions in the northern mid-latitudes (continued). Same as in Figure C4, for the regions E.Asia-W.Pacific and E.Pacific-NW.America.

https://doi.org/10.5194/egusphere-2026-7153
Preprint. Discussion started: 24 November 2026
© Author(s) 2026. CC BY 4.0 License.

References

Akritidis, D., Pozzer, A., Zanis, P., Tyrlis, E., Škerlak, B., Sprenger, M., and Lelieveld, J.: On the role of tropopause folds in summertime tropospheric ozone over the eastern Mediterranean and the Middle East, Atmospheric Chemistry and Physics, 16, 14 025–14 039, https://doi.org/10.5194/acp-16-14025-2016, 2016.

Appenzeller, C., Holton, J. R., and Rosenlof, K. H.: Seasonal variation of mass transport across the tropopause, Journal of Geophysical Research, 101, 15 071–15 078, https://doi.org/10.1029/96JD00821, 1996.

Banerjee, A., Chiodo, G., Previdi, M., Ponater, M., Conley, A., and Polvani, L.: Stratospheric water vapor: an important climate feedback, Climate Dynamics, https://doi.org/10.1007/s00382-019-04721-4, 2019.

Bozem, H., Joppe, P., Li, Y., Emig, N., Afchine, A., Breuninger, A., Curtius, J., Hofmann, S., Ismayil, S., Kandler, K., Kunkel, D., Kutschka, A., Lachnitt, H.-C., Petzold, A., Richter, S., Röschenthaler, T., Rolf, C., Schneider, L., Schneider, J., Vogel, A., and Hoor, P.: The TropoPause Composition TOwed Sensor Shuttle (TPC-TOSS): A new airborne dual platform approach for atmospheric composition measurements at the tropopause, EGUsphere [preprint], https://doi.org/10.5194/egusphere-2025-3175, 2025.

Butchart, N.: The Brewer-Dobson Circulation, Reviews of Geophysics, 52, 157–184, https://doi.org/10.1002/2013RG000448, 2014.

Bönisch, H., Hoor, P., Gurk, C., Feng, W., Chipperfield, M., Engel, A., and Bregman, B.: Model evaluation of CO_2 and SF_6 in the extratropical UT/LS region, Journal of Geophysical Research - Atmospheres, 113, https://doi.org/10.1029/2007JD008829, 2008.

Charlesworth, E., Plöger, F., Birner, T., Baikhadzhaev, R., Abalos, M., Abraham, N. L., Akiyoshi, H., Bekki, S., Dennison, F., Jöckel, P., Keeble, J., Kinnison, D., Morgenstern, O., Plummer, D., Rozanov, E., Strode, S., Zeng, G., Egorova, T., and Riese, M.: Stratospheric water vapor affecting atmospheric circulation, Nature Communications, 14, 3925, https://doi.org/10.1038/s41467-023-39559-2, 2023.

Clemens, J., Ploeger, F., Konopka, P., Portmann, R., Sprenger, M., and Wernli, H.: Climatology and variability of air mass transport from the boundary layer to the Asian monsoon anticyclone (ASMA) via shedding of low potential vorticity cutoffs, Atmospheric Chemistry and Physics, 22, 3841–3860, https://doi.org/10.5194/acp-22-3841-2022, 2022.

Dyroff, C., Zahn, A., Christner, E., Forbes, R., Tompkins, A. M., and van Velthoven, P. F. J.: Comparison of ECMWF analysis and forecast humidity data with CARIBIC upper troposphere and lower stratosphere observations, Quarterly Journal of the Royal Meteorological Society, 141, 833–844, https://doi.org/10.1002/qj.2400, 2015.

Emig, N., Miltenberger, A., Bozem, H., Krämer, M., Afchine, A., Kunkel, D., Lachnitt, H.-C., Li, Y., Reutter, P., Rolf, C., Spelten, N., Tost, H., and Hoor, P.: Turbulent mixing at the polar jet and transport of cirrus particles into the lowermost extratropical stratosphere, EGUsphere, 2026, 1–36, https://doi.org/10.5194/egusphere-2026-4614, 2026.

Fueglistaler, S., Dessler, A. E., Dunkerton, T. J., Folkins, I., Fu, Q., and Mote, P. W.: Tropical tropopause layer, Reviews of Geophysics, 47, RG1004, https://doi.org/10.1029/2008RG000267, 2009.

Gettelman, A., Hoor, P., Pan, L. L., Randel, W. J., Hegglin, M. I., and Birner, T.: The extratropical upper troposphere and lower stratosphere, Reviews of Geophysics, 49, https://doi.org/10.1029/2011RG000355, 2011.

Guo, Z. and Miltenberger, A.: Climatology of Warm Conveyor Belt Contributions to UTLS Moisture in ERA5 between 2010 and 2019, Journal of Climate, 38, 6505–6525, https://doi.org/10.1175/JCLI-D-25-0020.1, 2025.

Helten, M., Smit, H. G. J., Kley, D., Ovarlez, J., Schlager, H., Baumann, R., Schumann, U., Nedelec, P., and Marenco, A.: In-flight comparison of MOZAIC and POLINAT water vapor measurements, Journal of Geophysical Research: Atmospheres, 104, 26 087–26 096, https://doi.org/10.1029/1999JD900315, 1999.

https://doi.org/10.5194/egusphere-2026-7153
Preprint. Discussion started: 24 November 2026
© Author(s) 2026. CC BY 4.0 License.

Hersbach, H., Bell, B., Berrisford, P., Hirahara, S., Horányi, A., Muñoz-Sabater, J., Nicolas, J., Peubey, C., Radu, R., Schepers, D., Simmons, A., Soci, C., Abdalla, S., Abellan, X., Balsamo, G., Bechtold, P., Biavati, G., Bidlot, J., Bonavita, M., De Chiara, G., Dahlgren, P., Dee, D., Diamantakis, M., Dragani, R., Flemming, J., Forbes, R., Fuentes, M., Geer, A., Haimberger, L., Healy, S., Hogan, R. J., Hólm, E. A., Janisková, M., Keeley, S., Laloyaux, P., Lopez, P., Radnoti, G., Rosnay, P. D., Rozum, I., Vamborg, F., Villaume, S., and Thépaut, J.-N.: The ERA5 global reanalysis, Quarterly Journal of the Royal Meteorological Society, 146, 1999–2049, https://doi.org/10.1002/qj.3803, 2020.

Homeyer, C. R., Bowman, K. P., Smith, J. B., Ueyama, R., Dean-Day, J., Atlas, E., Smith, K., Pittman, J. V., Sayres, D., Wilmouth, D., Pandey, A., St. Clair, J. M., Hanisco, T. F., Hare, J., Hannun, R. A., Wofsy, S. C., Daube, B., and Donnelly, S.: Extreme Altitudes of Stratospheric Hydration by Midlatitude Tropopause-Overshooting Convection, Geophysical Research Letters, 50, e2023GL104 914, https://doi.org/10.1029/2023GL104914, 2023.

Homeyer, C. R., Gordon, A. E., Smith, J. B., Ueyama, R., Wilmouth, D. M., Sayres, D. S., Hare, J., Pandey, A., Hanisco, T. F., Dean-Day, J. M., Hannun, R., and Clair, J. M. S.: Stratospheric Hydration Processes in Tropopause-Overshooting Convection Revealed by Tracer-Tracer Correlations From the DCOTSS Field Campaign, Journal of Geophysical Research: Atmospheres, 129, e2024JD041 340, https://doi.org/10.1029/2024JD041340, 2024.

Hoor, P., Wernli, H., Hegglin, M., and Bönisch, H.: Transport timescales and tracer properties in the extratropical UTLS, Atmospheric Chemistry and Physics, 10, 7929–7944, https://doi.org/10.5194/acp-10-7929-2010, 2010.

Huang, Y., Wang, Y., and Huang, H.: Stratospheric Water Vapor Feedback Disclosed by a Locking Experiment, Geophysical Research Letters, 47, https://doi.org/10.1029/2020GL087987, 2020.

IPCC: Climate Change 2021 – The Physical Science Basis: Working Group I Contribution to the Sixth Assessment Report of the Intergovernmental Panel on Climate Change, https://doi.org/10.1017/9781009157896, 2023.

Jensen, E., Pfister, L., Park, M., and Ryoo, J.: Convective impact on the global lower stratospheric water vapor budget, Journal of Geophysical Research: Atmospheres, 129, e2023JD038 765, https://doi.org/10.1029/2023JD038765, 2024.

Jurkat-Witschas, T., Voigt, C., Groß, S., Kaufmann, S., Sauer, D., De la Torre Castro, E., Krämer, M., Schäfler, A., Afchine, A., Attinger, R., Bartolome Garcia, I., Beer, C. G., Bugliaro, L., Clemen, H., Dekoutsidis, G., Ehrlich, A., Grawe, S., Hahn, V., Hendricks, J., Järvinen, E., Klimach, T., Krüger, K., Krüger, O., Lucke, J., Luebke, A. E., Marsing, A., Mayer, B., Mayer, J., Mertes, S., Moser, M., Müller, H., Nenakhov, V., Pöhlker, M., Pöschl, U., Pörtge, V., Rautenhaus, M., Righi, M., Röttenbacher, J., Rubin-Zuzic, M., Schaefer, J., Schnaiter, M., Schneider, J., Schumann, U., Spelten, N., Stratmann, F., Tomsche, L., Wagner, S., Wang, Z., Weber, A., Wendisch, M., Wernli, H., Wetzel, B., Wirth, M., Zahn, A., Ziereis, H., and Zöger, M.: CIRRUS-HL: Picturing high- and mid-latitude summer cirrus and contrail cirrus above Europe with airborne measurements aboard the research aircraft HALO, Bulletin of the American Meteorological Society, 106, E2300–E2327, https://doi.org/10.1175/BAMS-D-23-0270.1, 2025.

Khordakova, D., Rolf, C., Grooß, J.-U., Müller, R. D., Konopka, P., Wieser, A., Krämer, M., and Riese, M.: A case study on the impact of severe convective storms on the water vapor mixing ratio in the lower mid-latitude stratosphere observed in 2019 over Europe, Atmospheric Chemistry and Physics, 22, 1059–1079, https://doi.org/10.5194/acp-22-1059-2022, 2022.

Konjari, P., Rolf, C., Hegglin, M. I., Rohs, S., Li, Y., Zahn, A., Bönisch, H., Nédélec, P., Krämer, M., and Petzold, A.: Technical note: Water vapour climatologies in the extra-tropical upper troposphere and lower stratosphere derived from a synthesis of passenger and research aircraft measurements, Atmospheric Chemistry and Physics, 25, 4269–4289, https://doi.org/10.5194/acp-25-4269-2025, 2025a.

https://doi.org/10.5194/egusphere-2026-7153
Preprint. Discussion started: 24 November 2026
© Author(s) 2026. CC BY 4.0 License.

Konjari, P., Rolf, C., Krämer, M., Afchine, A., Spelten, N., Bartolome Garcia, I., Miltenberger, A., Emig, N., Joppe, P., Schneider, J., Li, Y., Petzold, A., Bozem, H., and Hoor, P.: Stratospheric hydration and ice microphysics of a convective overshoot observed during the TPEx campaign over Sweden, Atmospheric Chemistry and Physics, 25, 18 031–18 050, https://doi.org/10.5194/acp-25-18031-2025, 2025b.

Konjari, P., Rolf, C., and Petzold, A.: IAGOS Adjusted Water Vapor Climatologies, https://doi.org/10.5281/zenodo.14852197, 2025c.

Kunkel, D., Hoor, P., Kaluza, T., Ungermann, J., Kluschat, B., Giez, A., Lachnitt, H.-C., Kaufmann, M., and Riese, M.: Evidence of small-scale quasi-isentropic mixing in ridges of extratropical baroclinic waves, Atmospheric Chemistry and Physics, 19, 12 607–12 630, https://doi.org/10.5194/acp-19-12607-2019, 2019.

Kunz, A., Sprenger, M., and Wernli, H.: Climatology of potential vorticity streamers and associated isentropic transport pathways across PV gradient barriers, Journal of Geophysical Research: Atmospheres, 120, 3802–3821, https://doi.org/https://doi.org/10.1002/2014JD022615, 2015.

Lachnitt, H.-C.: Consistent meteorological (ERA5) and chemical (CLaMS) information across airborne measurements over the globe between 1997 and 2023, https://doi.org/10.5281/zenodo.15076520, 2025.

Lambert, A., Read, W., and Livesey, N.: MLS/Aura Level 2 Water Vapor (H2O) Mixing Ratio V006, https://doi.org/10.5067/AURA/MLS/DATA2608, accessed: 2026-08-07, 2026.

McKenna, D. S., Konopka, P., Grooß, J.-U., Günther, G., Müller, R., Spang, R., Offermann, D., and Orsolini, Y.: A new Chemical Lagrangian Model of the Stratosphere (CLaMS) 1. Formulation of advection and mixing, Journal of Geophysical Research: Atmospheres, 107, ACH 15–1–ACH 15–15, https://doi.org/https://doi.org/10.1029/2000JD000114, 2002.

Neis, P., Smit, H., Rohs, S., Bundke, U., Krämer, M., Spelten, N., Ebert, V., Buchholz, B., Thomas, K., and Petzold, A.: Quality assessment of MOZAIC and IAGOS capacitive hygrometers: Insights from airborne field studies, Tellus B, 67, https://doi.org/10.3402/tellusb.v67.28320, 2015.

Pepler, A. S. and Dowdy, A. J.: Fewer deep cyclones projected for the midlatitudes in a warming climate, but with more intense rainfall, Environmental Research Letters, 16, 054 044, https://doi.org/10.1088/1748-9326/abf528, 2021.

Pettegrew, B. P., Market, P. S., Wolf, R. A., Holle, R. L., and Demetriades, N. W. S.: A Case Study of Severe Winter Convection in the Midwest, Weather and Forecasting, 24, 121–139, https://doi.org/10.1175/2008WAF2007103.1, 2009.

Petzold, A., Thouret, V., Gerbig, C., Zahn, A., Brenninkmeijer, C., Gallagher, M., Hermann, M., Pontaud, M., Ziereis, H., Boulanger, D., Marshall, J., Nédélec, P., Smit, H., Frieß, U., Flaud, J.-M., Wahner, A., Cammas, J.-P., and Volz-Thomas, A.: Global-scale atmosphere monitoring by in-service aircraft - current achievements and future prospects of the European Research Infrastructure IAGOS, Tellus B, 67, https://doi.org/10.3402/tellusb.v67.28452, 2015.

Ploeger, F., Günther, G., Konopka, P., Fueglistaler, S., Müller, R., Hoppe, C., Kunz, A., Spang, R., Grooß, J.-U., and Riese, M.: Horizontal water vapor transport in the lower stratosphere from subtropics to high latitudes during boreal summer, Journal of Geophysical Research: Atmospheres, 118, 8111–8127, https://doi.org/10.1002/jgrd.50636, 2013.

Reutter, P., Škerlak, B., Sprenger, M., and Wernli, H.: Stratosphere–troposphere exchange (STE) in the vicinity of North Atlantic cyclones, Atmospheric Chemistry and Physics, 15, 10 939–10 953, https://doi.org/10.5194/acp-15-10939-2015, 2015.

Riese, M., Ploeger, F., Rap, A., Vogel, B., Konopka, P., Dameris, M., and Forster, P.: Impact of uncertainties in atmospheric mixing on simulated UTLS composition and related radiative effects, J. Geophys. Res., 117, D16 305, https://doi.org/10.1029/2012JD017751, 2012.

Rolf, C., Afchine, A., Bozem, H., Buchholz, B., Ebert, V., Guggenmoser, T., Hoor, P., Konopka, P., Kretschmer, E., Müller, S., Schlager, H., Spelten, N., Sumińska-Ebersoldt, O., Ungermann, J., Zahn, A., and Krämer, M.: Transport of Antarctic stratospheric strongly dehydrated

https://doi.org/10.5194/egusphere-2026-7153
Preprint. Discussion started: 24 November 2026
© Author(s) 2026. CC BY 4.0 License.

air into the troposphere observed during the HALO-ESMVal campaign 2012, Atmospheric Chemistry and Physics, 15, 9143–9158, https://doi.org/10.5194/acp-15-9143-2015, 2015.

Rolf, C., Rohs, S., Smit, H., Krämer, M., Bozóki, Z., Hofmann, S., Franke, H., Maser, R., Hoor, P., and Petzold, A.: Evaluation of compact hygrometers for continuous airborne measurements, Meteorologische Zeitschrift, pp. –, https://doi.org/10.1127/metz/2023/1187, 2023.

Schoeberl, M. R., Douglass, A. R., Hilsenrath, E., Bhartia, P. K., Beer, R., Waters, J. W., Gunson, M. R., Froidevaux, L., Gille, J. C., Barnett, J. J., Levelt, P. F., and DeCola, P.: Overview of the EOS Aura Mission, IEEE Transactions on Geoscience and Remote Sensing, 44, 1066–1074, https://doi.org/10.1109/TGRS.2005.861950, 2006.

Schwenk, C. and Miltenberger, A.: The role of ascent timescales for warm conveyor belt (WCB) moisture transport into the upper troposphere and lower stratosphere (UTLS), Atmospheric Chemistry and Physics, 24, 14 073–14 099, https://doi.org/10.5194/acp-24-14073-2024, 2024.

Solomon, S., Rosenlof, K., Portmann, R., Daniel, J., Davis, S., Sanford, T., and Plattner, G.-K.: Contributions of Stratospheric Water Vapor to Decadal Changes in the Rate of Global Warming, Science (New York, N.Y.), 327, 1219–23, https://doi.org/10.1126/science.1182488, 2010.

Sprenger, M. and Wernli, H.: A northern hemispheric climatology of cross-tropopause exchange for the ERA15 time period (1979–1993), Journal of Geophysical Research: Atmospheres, 108, https://doi.org/10.1029/2002JD002636, 2003.

Szakáll, M., Mohácsi, , Tátrai, D., Szabó, A., Huszár, H., Ajtai, T., Szabó, G., and Bozóki, Z.: Twenty Years of Airborne Water Vapor and Total Water Measurements of a Diode Laser Based Photoacoustic Instruments, Frontiers in Physics, 8, 384, https://doi.org/10.3389/fphy.2020.00384, 2020.

Vömel, H., David, D. E., and Smith, K.: Accuracy of Tropospheric and Stratospheric Water Vapor Measurements by the Cryogenic Frost Point Hygrometer: Instrumental Details and Observations, Journal of Geophysical Research: Atmospheres, 112, D08 305, https://doi.org/10.1029/2006JD007224, 2007.

Vömel, H., Naebert, T., Dirksen, R., and Sommer, M.: An update on the uncertainties of water vapor measurements using cryogenic frost point hygrometers, Atmospheric Measurement Techniques, 9, 3755–3768, https://doi.org/10.5194/amt-9-3755-2016, 2016.

Wang, H., Park, M., Tao, M., Peña-Ortiz, C., Plaza-Martin, N. P., Ploeger, F., and Konopka, P.: Understanding boreal summer UTLS water vapor variations in monsoon regions: a Lagrangian perspective, Atmospheric Chemistry and Physics, 25, 14 703–14 718, https://doi.org/10.5194/acp-25-14703-2025, 2025.

Zahn, A., Brenninkmeijer, C. A. M., and van Velthoven, P. F. J.: Passenger aircraft project CARIBIC 1997–2002, Part I: the extratropical chemical tropopause, Atmospheric Chemistry and Physics Discussions, 4, 1091–1117, https://doi.org/10.5194/acpd-4-1091-2004, 2004.

Zahn, A., Christner, E., Velthoven, P., Rauthe-Schöch, A., and Brenninkmeijer, C.: Processes controlling water vapor in the upper troposphere/lowermost stratosphere: An analysis of 8 years of monthly measurements by the IAGOS-CARIBIC observatory: CARIBIC H2O in the UT/LMS, Journal of Geophysical Research: Atmospheres, 119, https://doi.org/10.1002/2014JD021687, 2014.

Zöger, M., Afchine, A., Eicke, N., Gerhards, M.-T., Klein, E., McKenna, D. S., Mörschel, U., Schmidt, U., Tan, V., Tuitjer, F., Woyke, T., and Schiller, C.: Fast in situ stratospheric hygrometers: A new family of balloon-borne and airborne Lyman α photofragment fluorescence hygrometers, Journal of Geophysical Research: Atmospheres, 104, 1807–1816, https://doi.org/10.1029/1998JD100025, 1999.